

POSSIBLE SOLUTIONS TO THE RADIUS ANOMALIES OF TRANSITING GIANT PLANETS

A. BURROWS¹, I. HUBENY¹, J. BUDAJ^{1,2}, & W.B. HUBBARD³

Accepted to Ap.J. February 9, 2007

ABSTRACT

We calculate the theoretical evolution of the radii of all fourteen of the known transiting extrasolar giant planets (EGPs) for a variety of assumptions concerning atmospheric opacity, dense inner core masses, and possible internal power sources. We incorporate the effects of stellar irradiation and customize such effects for each EGP and star. Looking collectively at the family as a whole, we find that there are in fact two radius anomalies to be explained. Not only are the radii of a subset of the known transiting EGPs larger than expected from previous theory, but many of the other objects are smaller than the default theory would allow. We suggest that the larger EGPs can be explained by invoking enhanced atmospheric opacities that naturally retain internal heat. This explanation might obviate the necessity for an extra internal power source. We explain the smaller radii by the presence in perhaps all the known transiting EGPs of dense cores, such as have been inferred for Saturn and Jupiter. Importantly, we derive a rough correlation between the masses of our “best-fit” cores and the stellar metallicity that seems to buttress the core-accretion model of their formation. Though many caveats and uncertainties remain, the resulting comprehensive theory that incorporates enhanced-opacity atmospheres and dense cores is in reasonable accord with all the current structural data for the known transiting giant planets.

Subject headings: stars: transits — planetary systems — planets and satellites: general

1. INTRODUCTION

Approximately two hundred extrasolar giant planets (EGPs) have to date been discovered by radial-velocity techniques⁴. These data yield orbital properties and $M_p \sin(i)$, where M_p and i are the planet mass and inclination angle, respectively. However, for the subset of fourteen EGPs that are currently known to transit their primaries (Charbonneau et al. 2006a), the $M_p - \sin(i)$ degeneracy is broken and EGP radii (R_p) are measured as well. With M_p and R_p , an estimate of the (presumably) coeval stellar age, and a detailed theoretical model that includes the effects of stellar irradiation, the general theory of the structure, evolution, and atmospheres of irradiated close-in EGPs⁵ can be put to the test (Burrows et al. 2000; Bodenheimer, Lin, & Mardling 2001; Bodenheimer, Laughlin, & Lin 2003; Burrows, Sudarsky, & Hubbard 2003; Baraffe et al. 2003; Burrows et al. 2004; Chabrier et al. 2004; Laughlin et al. 2005; Baraffe et al.

2005).

Recently, observers and theorists alike have focussed on the apparent discrepancy with published theory of the transit radii of some EGPs, notably HD209458b, HAT-P-1b, and WASP-1b (Knutson et al. 2006; Bakos et al. 2006b; Charbonneau et al. 2006c), i.e. that these close-in EGPs are larger than most theories would predict. Many would explain this anomaly by invoking an extra heat source for the interior, perhaps caused by orbital tidal forcing (Bodenheimer, Laughlin, & Lin 2003), obliquity tides when in a Cassini state (Winn & Holman 2005), or penetration of gravity waves into the planetary interior that then dissipate at depth (Guillot & Showman 2002; Showman & Guillot 2002). Such a power source could indeed be operative, and the powers required are not large (§7). However, the transit radius of an EGP depends upon M_p , the stellar flux at the planet (F_p , §3), its atmospheric composition (§5), the possible presence of an inner core (§6), its age, and the atmospheric circulation that couples the day and the night sides (§8). It also depends upon the fact that the transit line of sight cuts the chord of the planet, and not its radial profile (§4). This effect can add ~3% to ~10% to the measured radius (Burrows, Sudarsky, & Hubbard 2003; Burrows et al. 2004; Baraffe et al. 2003) and should be included in a detailed comparison with observation.

With so many determinants of a planet’s radius, comparison between theory and measurement must be multi-parametric. Furthermore, errors in the measured R_p and M_p , in the ages, and in the stellar metallicities can be large. These introduce significant noise in the interpretation of any one transiting EGP and are why it is more fruitful to look broadly at the entire family. In this way, we are able to determine the overall systematics in the structures of close-in EGPs and discover trends and characteristics that would otherwise be obscured if we had

¹ Department of Astronomy and Steward Observatory, The University of Arizona, Tucson, AZ 85721; burrows@zenith.as.arizona.edu, budaj@as.arizona.edu, hubeny@aegis.as.arizona.edu

² Astronomical Institute, 05960 Tatranska Lomnica, Slovak Republic

³ Department of Planetary Sciences and the Lunar and Planetary Laboratory, The University of Arizona, Tucson, AZ 85721; hubbard@lpl.arizona.edu

⁴ see J. Schneider’s Extrasolar Planet Encyclopaedia at <http://www.obspm.fr/encycl/encycl.html> and the Carnegie/California compilation at <http://exoplanets.eu>.

⁵ We will not use the term “Hot Jupiters,” since it is a misnomer from the point of view of spectra and atmospheres. The hallmarks of Jupiter’s atmosphere, cold ammonia and water clouds and methane gas, could not survive in the extreme irradiation regime of a close-in EGP that experiences ~10⁴ times higher fluxes and has atmospheric temperatures that are an order of magnitude hotter. In the atmospheres of the known transiting EGPs, carbon is in carbon monoxide, alkali metals, not seen in Jupiter, are the predominant absorbers at optical wavelengths, and water is steam.

focused on one object at a time. As a result, we put less weight on our object-by-object “best-fits” than in the patterns that emerge from our study of them collectively.

We find that the range of observed radii for the entire cohort of transiting EGPs is too large to accommodate only one radius anomaly. We show, in fact, that some (most) transiting EGPs are *smaller* than past theory would have predicted, while we confirm that some are larger than past theory would have predicted. We can explain both anomalies with 1) enhanced atmospheric opacities for the larger EGPs and 2) “ice/rock” cores for the smaller EGPs. Such cores are predicted by the “core-accretion” model of giant planet formation (Pollack et al. 1996) and ice/rock cores shrink an EGP of a given total mass monotonically with core mass. An extreme case is HD149026b (Charbonneau et al. 2006b; Fortney et al. 2006). Interestingly, we derive a rough correlation between the inferred core masses and the parent star metallicity. This trend suggests their origin.

Larger atmospheric abundances, such as those measured for Jupiter and Saturn (§5; Atreya et al. 2003; Atreya 2006; Flasar et al. 2005), would lead naturally to larger atmospheric opacities that retard the loss of heat and entropy from an EGP and delay the shrinkage of its radius. However, in this paper we are not tying such enhanced atmospheric opacities solely to enhanced atmospheric abundances/metallicities. This is an important point. Rather, we are suggesting that the atmospheres of close-in EGPs could also be altered significantly by strong optical and UV irradiation. The thick hazes, absorbing clouds, and non-equilibrium chemical species that could thereby be produced might lead to significant increases in the optical thickness of the atmospheric blanket, leading to a slowdown in the rate of loss of core heat. Enhanced atmospheric opacity has an effect similar to extra core power. We note that the UV flux at the surface of the transiting planets is as much as a factor of 10^4 times higher than that at the surface of Jupiter. Despite the much lower Jovian UV insolation, its atmosphere contains as-yet-identified trace non-equilibrium species at the part in $\sim 10^{10}$ level that nevertheless result in a decrease by almost a factor of *two* in its blue and green geometric albedos. What might be the response in the atmosphere of a close-in EGP to the factor of 10^4 increase in UV irradiation?

Therefore, in this paper we explore the consequences for EGP radii of enhanced atmospheric opacities. We do this by calculating models using solar, $3\times$ solar, and $10\times$ solar abundance atmospheres, but the latter two should be considered ersatz for the effects of enhanced opacities of whatever origin. Hence, we decouple the effects of increased atmospheric opacity from increased envelope heavy-element abundances. If the increase in atmospheric opacity were due solely to increased metallicity and our equilibrium chemistry and opacity algorithms were correct, then the implied increases in the heavy-element burden of the envelope, if the heavy fraction in both atmosphere and envelope were the same, could partially or wholly cancel the expansion effect of enhanced atmospheric opacity (see §6 and Fig. 8). We leave open the detailed reasons for the enhanced opacities, which could, in addition to super-solar metallicities in the atmosphere, be non-equilibrium chemistry, errors

in the default opacities, and/or thick hazes or clouds. In the near future, measurements of both the reflected light and thermal emission of close-in EGPs should help to constrain both the opacities and compositions of their atmospheres. We note that the detection by Charbonneau et al. (2002) of sodium in the atmosphere of HD209458b is best fit by the presence of hazes (Fortney et al. 2003) or some additional grayish absorber. The default theory using clear atmospheres does not explain the factor-of-three discrepancy (from merely solar!) in the inferred abundance of sodium in HD209458b’s atmosphere.

The upshot of these dual themes concerning atmospheres and cores is a theory that might explain all the transit radii without resorting to an extra power source to inflate them. Though an extra power source is still possible, we find no simple correlation between the magnitude of the needed power and any planetary or stellar properties.

In §2, we review the transit data and summarize their interesting features, particularly those that demand special explanation. Section 3 demonstrates the general dependence of transit radii on M_p and stellar flux (F_p). The latter varies by more than an order of magnitude among the known transiting EGPs. In §4, we discuss the “transit-radius” effect that arises from the fact that we measure an impact parameter and not a radius. In §5, we present the results of our calculations without cores for solar-opacity and $10\times$ solar-opacity atmospheres. These models are the baseline suite that set the stage for the discussions that follow⁶. The higher opacity models can fit the large-radius EGPs, modulo remaining uncertainties in their ages. We note again that we use increased atmospheric metallicity as a convenient substitute for enhanced opacity. In §6, we discuss the effects of a central “ice/rock” core and calculate a range of core masses needed to achieve better fits for the relevant EGPs. This section motivates a possible correlation between the inferred core masses and the stellar metallicity that might inform models of their formation. In §7, we discuss the possible effect on planet structure of an extra heat source and determine how much power, object by object, would be needed to explain the measured R_p s for simple models of planet cooling. This section is meant merely to provide the reader with a gauge of the range of powers that might be required should our default and preferred set of models be shown in the future to fail in some crucial particular. Curiously, we find that inner cores are still suggested by the data even when an extra internal heat source is present. In §8, we discuss a major theoretical uncertainty – the advection of heat from the day to the night sides due to global circulation. Atmospheric winds at altitude and at depth remain wild cards in the general theory of EGPs. In §9, we summarize our results and conclusions and reiterate the remaining caveats concerning the theory of EGP radii.

2. MEASUREMENTS OF CLOSE-IN GIANT PLANETS

Table 1 is a compilation of relevant data for the fourteen known transiting planets, listed in order of increasing semi-major axis. These data include semi-major axis

⁶ We have also calculated $3\times$ solar-opacity models to better determine the opacity dependence of transit radii and provide a more comprehensive view, but do not provide the corresponding plots.

(a), period (P), M_p , R_p , F_p , and recent observational references. We also provide the latest error bars for M_p and R_p , though when it seemed prudent we have rounded both these and the central estimates. Note that the flux at the planet is not monotonic with orbital distance, reflecting the fact that these EGPs orbit a variety of stars with luminosities that span an order of magnitude. Table 2 provides these luminosities (L_*), along with other useful stellar parameters, such as spectral type, stellar radius (R_*), effective temperature (T_{eff}), surface gravity (g), metallicity ($[\text{Fe}/\text{H}]$), and stellar mass (M). We also provide in Table 2 the system distances; some (such as those for the OGLE set) are quite approximate. Most of the data in Tables 1 and 2 are necessary to construct theoretical models and compare them with the measurements. For instance, to incorporate the effects of stellar irradiation one needs models of the stellar spectra and luminosities. We employed those of Kurucz (1994), or generated our own using the atmosphere code TLUSTY (Hubeny & Lanz 1995). In Table 2, we include ages and their error bars, both of which should be considered very approximate. We list only the central guesses of the stellar metallicities given in the literature, but ample error bars for them should also be assumed. The ages and the metallicities are the least well-known quantities in Table 2 and ambiguities in them translate into uncertainties in the interpretation of the theoretical models and transit data for any given object. However, as Table 2 suggests, the metallicities of these EGP parents vary by a factor of ~ 4 . The ages probably range even more broadly.

Figure 1 depicts R_p versus M_p for all the transiting EGPs given in Table 1, along with error bars. Jupiter and Saturn are included for context. This figure encapsulates the basic measurements to be explained by theory and warrants some discussion. The first thing to note is that the spread in transit radii is wide, $\sim 40\%$ for the bulk and approximately a factor of two when HD149026b is included. Some have noted that there is a tendency for the larger EGPs to be orbiting the more massive primary stars (see Table 2). This is most easily explained by the fact that such stars have higher luminosities, and, hence, that their EGPs find themselves in more intense irradiation regimes (all else being equal), but planet/star distance and planet mass also play central roles. In fact, the largest values of F_p are for OGLE-TR-56b, OGLE-TR-132b, and WASP-1b, while HD209458b and TrES-2 are in the middle of the pack (see Table 1). As the upper envelope of the data in Fig. 1 suggests, there is a slight tendency for the lower mass EGPs to have higher radii. This effect is a straightforward consequence of basic theory and is at least as important (§3).

There are other apparent curiosities. Using Fig. 1 and Table 1, we can compare subsets of EGPs with roughly the same M_p . One such triplet, in order of decreasing radius, is WASP-1b, XO-1b, and WASP-2b. We might expect that, given this radius hierarchy, F_p would monotonically decrease from WASP-1b to WASP-2b. However, F_p for XO-1b is lower than that for WASP-2b. HAT-P-1b, OGLE-TR-10b, and OGLE-TR-111b constitute a similar triplet, but F_p for OGLE-TR-111b is the largest of the three, breaking what should otherwise be a monotonic trend. Moreover, the radii and masses of HD189733b and OGLE-TR-132b are roughly the same, yet their F_p s are almost an order of magnitude differ-

ent. The most extreme case is HD149026b, which has the fourth highest F_p , but the smallest radius. Our overall thesis is that these features can be explained, to within the error bars, not one-dimensionally, but only after the various effects of M_p , F_p , core mass, atmospheric opacity, and age are simultaneously addressed.

Figure 2 depicts the dependence of the measured R_p on the estimates of the stellar metallicity ($[\text{Fe}/\text{H}]$, Table 2). Error bars in both quantities, in particular $[\text{Fe}/\text{H}]$, will smear this plot, but the basic relationships, if there are any, should emerge as plotted. We see that at all metallicities, there is a wide range of measured radii, and no clear and simple correlation with either M_p or F_p (Table 1). Curiously, there seem to be two branches (upper and lower), but this may be an artefact of small-number statistics. In any case, Figs. 1 and 2 and Tables 1 and 2 summarize the salient information concerning the known transiting EGPs to be explained by theory.

3. DEPENDENCE ON STELLAR FLUX AND M_p

To demonstrate the general dependence of R_p upon orbital distance and M_p , we have generated Fig. 3. In it, we depict evolutionary trajectories for a Saturn-mass planet ($0.3 M_J$ ⁷, solid) and a Jupiter-mass planet (dashed) at distances from a G2V main sequence star of 0.02, 0.03, 0.04, 0.05, and 0.06 AU. These models are not per se our preferred models for any of the known transiting EGPs, assume solar-metallicity atmospheric abundances (Asplund, Grevesse, & Sauval 2006) and opacities, do not include inner cores, but, as do all the models we present in this paper, employ the well-developed boundary condition formalism of Burrows, Sudarsky, & Hubbard (2003) and Burrows et al. (2004). For these, and all evolutionary calculations in this paper, we pre-calculate grids of self-consistent irradiation boundary conditions at 130 points that span the internal flux and surface gravity space (Burrows, Sudarsky, & Hubbard 2003) likely to be traversed during the evolution of each single primary star/semi-major-axis combination. During each evolutionary calculation, we interpolate in this grid of boundary conditions. Appropriately different stellar spectra (see Table 2; Kurucz 1994; Hubeny & Lanz 1995) for each system are employed and we set up these grids for each of the 14 known transiting EGPs and three sets of opacities (§5). Hence, for this study we have calculated $14 \times 130 \times 3 = 5460$ detailed spectral/atmosphere models.

We see immediately that the radius of a low-mass EGP is more sensitive to distance, with that of a Saturn-mass EGP varying by $\sim 0.2 R_J$ ⁸ from 0.02 AU to 0.06 AU and that of a more-massive Jupiter-mass EGP varying by $\sim 0.1 R_J$ over the same orbital distance range. Moreover, younger EGPs have larger radii than older representatives, but after ~ 1.0 Gyr all evolutionary trajectories start to flatten. This fact emphasizes the potential role of youth in providing large radii, and the ambiguities that arise in the interpretation of transiting EGPs with poorly-known ages. This is particularly relevant for OGLE-TR-111b, HD189733b, TrES-2, WASP-1b, and WASP-2b, whose ages are either unknown or very poorly known. Figure 3 also shows that the timescale for radius decay is longer for lower-mass EGPs.

⁷ $1 M_J$ (Jupiter's mass) $\equiv 1.89914 \times 10^{30}$ g

⁸ $1 R_J$ (the radius of Jupiter) $\equiv 7.15 \times 10^9$ cm

Figure 4 continues our demonstration of the effects of irradiation and planet mass on R_p by depicting its direct dependence on the stellar flux (F_p) at the substellar point for the same class of theoretical models. Roughly one order of magnitude in F_p is depicted. Masses of 0.3, 0.5, 0.65, 1.0, and 1.25 M_J are shown for an age of 2.5 Gyr. This age is roughly the mean age of stars in the solar neighborhood. Again, we see that, all else being equal, smaller-mass EGPs have larger radii and depend more steeply upon F_p . For a 1.25- M_J EGP, R_p varies for the depicted range of F_p s by $\sim 0.08 R_J$, while for a 0.3- M_J EGP it varies by as much as $\sim 0.24 R_J$. This behavior is consonant with our statement in §2 that the upper envelope of the data depicted in Fig. 1 has a negative slope. Note that the spread in R_p with mass at high F_p is significantly larger than at low F_p . This is connected with the convergence of the radii of cold EGPs due to the $n = 1$ polytropic character of the H_2/He equation of state (Burrows et al. 2001).

4. TRANSIT RADIUS EFFECT

Measuring a transit provides the impact parameter of the planet, not its photospheric radius. This means that the planetary limb, through which the light from the star that defines the depth of the transit emerges, is at a slightly larger distance from the projected planet center than the canonical $\tau = 2/3$ planetary radius. For large F_p s, high atmospheric metallicities, and small M_p , this difference can be $\sim 5\%$. Hence, the effect should be included in any comparison with data and failure to include it will exaggerate the apparent discrepancy with the previous theory of the radii of the biggest transiting EGPs. For the 0.64- M_J EGP HD209458b, the effect can be larger than 0.05 R_J (Burrows, Sudarsky, & Hubbard 2003; Baraffe et al. 2003).

The wavelength-dependent optical depth, τ_{chord} , along a chord followed by the stellar beam through the planet’s upper atmosphere, is approximately:

$$\tau_{\text{chord}} \sim \kappa \rho_{ph} H \sqrt{\frac{2\pi R_p}{H}} e^{-\left(\frac{\Delta R_{ch}}{H}\right)}, \quad (1)$$

where κ is the wavelength-dependent opacity, ρ_{ph} is the mass density at the photosphere, ΔR_{ch} is the excess radius over and above the $\tau_{ph} = \frac{2}{3}$ radius (the radius of the traditional photosphere), and H is the atmospheric density scale height. The latter is given approximately by $kT/\mu g m_p$, where μ is the mean molecular weight, g is the surface gravity, T is some representative atmospheric temperature, and m_p is the proton mass. By definition, and assuming an exponential atmosphere, $\tau_{ph} = \kappa \rho_{ph} H = \frac{2}{3}$. For τ_{chord} to equal $\frac{2}{3}$, this yields

$$\Delta R_{ch} = H \ln \sqrt{\frac{2\pi R_p}{H}} \sim 5 H. \quad (2)$$

ΔR_{ch} should be included in the theoretical radius that is compared with the measured transit radius. In this paper, we include it implicitly by first calculating the radius of the convective-radiative boundary and then adding to it the additional distance to the $\tau_{\text{chord}} = 2/3$ level in the corresponding detailed atmosphere model. We refer to this additional distance as ΔR (no subscript), which contains ΔR_{ch} . Figure 6 depicts ΔR versus planet

mass (Table 1) for solar (black) and 10×solar (red) atmospheric opacities and representative coreless models of twelve of the measured transiting EGPs. The distance, ΔR , from the radiative-convective boundary to the $\tau_{\text{chord}} = 2/3$ level is between $\sim 0.04 R_J$ and $\sim 0.15 R_J$ for H_2/He -dominated atmospheres, depending mostly on the planet’s mass (M_p), the stellar flux at the planet (F_p), and (weakly) its age. As Fig. 5 indicates, ΔR is smaller for higher-mass EGPs, larger for planets experiencing higher F_p s (see Table 1), and larger for higher atmospheric opacities. Concerning the latter, the increase in ΔR in going from solar to 10×solar ranges from ~ 0.01 to $\sim 0.04 R_J$. The contribution of ΔR_{ch} to ΔR varies from $\sim 10\%$ to $\sim 50\%$. Note that the numbers depicted in Fig. 5 assume that the mean molecular weight (μ) is not altered at high opacity. Even if high opacity meant high metallicity, the μ effect at 10×solar would amount to a diminution of the scale height and the transit-radius effect itself by no more than $\sim 20\%$ of the enhancement, and would not compensate for the corresponding increase in ΔR due to the opacity effect.

5. MODELS WITH SOLAR- AND ENHANCED-OPACITY ATMOSPHERES AND NO CORES

In situ and remote-sensing measurements of the atmospheric compositions of the giant planets Jupiter and Saturn reveal that most of the dominant elements, such as carbon, nitrogen, and sulfur, exist there in super-solar abundances (Atreya et al. 2003). Atreya (2006) estimates that $[N/H]$ and $[C/H]$ in Jupiter’s atmosphere are 4-5 times solar and that $[C/H]$ in Saturn’s atmosphere is 9-10 times solar. Furthermore, Flasar et al. (2005) estimate that carbon in Saturn’s atmosphere is ~ 7 times solar. Given the ambiguities in the interpretation of the Galileo probe results, $[O/H]$ is problematic, but it too is widely considered to be super-solar. Since the metallicities of EGP host stars are preferentially in excess of the Sun’s (Fischer & Valenti 2005), the idea that the atmospheres of orbiting EGPs are heavy-element-rich is more than just an intriguing possibility. In addition, the excesses seen in Jupiter and Saturn are in keeping with the core-accretion model of giant planet formation (Pollack et al. 1996), and are some of the reasons it is preferred.

It was these super-solar heavy-element abundances in the Jovian planets that first motivated us to explore the effects on EGP radii of enhanced atmospheric opacities. As we suggest in §1, even for solar abundances, strong irradiation may significantly alter the chemistry and opacities of the atmospheres of close-in EGPs. Hereafter, we use super-solar metallicity as a substitute for enhanced opacity by whatever means and for whatever elemental abundance pattern and metallicity. We explore the consequences for the radii of irradiated EGPs of such opacities and compare with the corresponding results for default solar-metallicity atmospheres. In the models that follow, 3×solar and 10×solar are to mean “with heavy-element opacities that are 3 and 10 times what they would be at a given temperature and pressure for the canonical, unaltered solar-metallicity atmosphere.” However, note that the envelopes of the models presented here are assumed to be pure H/He mixtures and that the effect on the planet’s radius of envelope metals is, for our purposes, “absorbed” into an effect due to the core alone. Hence, our cores “stand in” for

the core/envelope vis à vis their summed effect on the planet radius (§6).

Higher atmospheric opacities retain the core’s heat and entropy, and this maintains the EGP’s radius at higher values for longer times. This consequence of higher atmospheric gas-phase opacities (which could be abetted by upper atmosphere clouds; cf. Fortney et al. 2003) is similar in effect to that of an extra core power source (§7), but we believe that this explanation of large EGP radii may be more natural.

As stated in §3, for all our calculations, we employ the evolutionary, spectral, atmospheric, and opacity techniques described in Burrows, Sudarsky, & Hubbard (2003) and Hubeny, Burrows, & Sudarsky (2003), and discussed in Burrows et al. (2001)⁹. We set the redistribution factor (Burrows et al. 2004), f , equal to 1/4, and, therefore, assume complete heat redistribution at depth (see §8). Figures 6 and 7 portray theoretical evolutionary trajectories of R_p versus age for coreless models of all fourteen of the known transiting EGPs. Model atmospheres for both solar opacity (top) and 10×solar opacity (bottom) are shown and models with (right) and without (left) the ΔR term are included for comparison. The measured transit radii and ages are superposed, along with error bars (Tables 1 and 2). For each EGP, the color used for both model and data is the same. Since the ages for WASP-1b and WASP-2b are not in the literature, we arbitrarily set them equal to 2 ± 1 Gyrs.

Figure 6 contains eight of the smallest measured EGPs, and Fig. 7 contains the other six (and, hence, the largest) EGPs. The cut between the two sets is of no fundamental significance. As Fig. 6 indicates, if we use solar opacities, ignore ΔR , and leave out a core, the left-hand-side models would fit the corresponding data rather well, except for HD149026b. All the coreless models of HD149026b are discrepant by wide margins (by as much as a factor of two) and a core of substantial mass seems the only option (Fortney et al. 2006; §6). In fact, HD149026b is more like a super-Neptune than an EGP.

The wide range of possible ages for some of the EGPs depicted in Fig. 6, in particular for OGLE-TR-111b and OGLE-TR-113b, makes interpretation a bit uncertain, particularly in the lower age range. However, for longer ages the models are substantially age-independent. In addition, one can’t arbitrarily ignore the ΔR term and as the top right-hand panel of Fig. 6 indicates, the solar/coreless “fits” then evaporate when including it. Even if the errors in R_p are obliging, and data and model for a few of the eight EGPs are reconciled, one is unlikely to be able to do this for all of them. The upshot is that even at solar opacities coreless models for these smaller transiting EGPs are disfavored. Models portrayed in the 10×solar panels at the bottom of Fig. 6 are even more disfavored. The actual opacities of the atmospheres of these EGPs don’t have to be as high as for the 10×solar models for these plots to be indicative of a severe problem. This is the first major radius problem: many of the known transiting EGPs are too small, not too large.

Figure 7 depicts the six largest transiting EGPs in the same format as Fig. 6. The gap with theory for solar opacities, no cores, and no ΔR term is wide for all,

except for TrES-2, if its age is quite low. As the upper right-hand panel indicates, including the ΔR effect helps, but not enough. However, at $\sim 10\times$ solar, the models for all these larger EGPs start to fit rather well, the degree of fit depending centrally upon the age and radius error bars. In fact, for OGLE-TR-10b and OGLE-TR-56b, their 10×solar-opacity radii are on average *too* large. This is true for OGLE-TR-56b, despite its large F_p (Table 1). The measured radius of HD209458b is still a bit larger than the theory, but it is within $1.5\text{-}\sigma$ for its central age estimate, and better than this for younger ages. HAT-P-1b fits well, TrES-2 fits well for a wide range of ages. WASP-1b can fit, in particular if it is not very old (recall that its age is unknown). The largest opacity effects, those associated with an increase in radius of $\sim 0.05\text{-}0.1 R_J$ in going from solar to 10×solar, obtain for the least massive EGPs (lowest M_p s) with the highest irradiation fluxes, F_p s (see Table 1). For HD149026b, for which $M_p = 0.36 M_J$ and F_p is the fourth highest, the magnitude of the atmospheric opacity enhancement effect is $\sim 0.2 R_J$.

Therefore, we conclude that higher-opacity atmospheres and the inclusion of the ΔR term can explain the largest of the measured radii. Moreover, the range of radii among the fourteen known transiting EGPs is too wide to be explained by one factor alone. Importantly, there is a small-radius problem as well, one that can not be solved by an extra heat source. We next show in §6 that ice-rock cores for almost all the known EGPs, with smaller cores for the largest EGPs, are indicated.

6. EFFECT OF A CENTRAL CORE

In the core-accretion model of giant planet formation (Pollack et al. 1996), a mass of ice and rock accumulates until it achieves a critical mass. This critical mass then nucleates rapid gas accretion and the giant planet grows to its final mass at the expense of the surrounding protostellar nebula. Such a two-step process is suggested because nebular temperatures are estimated to be too high for the inferred disk areal mass densities to allow direct gravitational instability by the Toomre condition (Boss 1997, 2001), akin to the Jeans criterion for star formation. Importantly, there is direct evidence for the presence of a ~ 15 Earth-mass¹⁰ core in Saturn and some evidence for a similar core in Jupiter (Guillot & Saumon 2004). The ice giants Neptune (17.1 Earth masses) and Uranus (14.5 Earth masses) are thought to be such nuclei that may have been starved of gas at birth by the low-density neighborhood in which they were born.

In all cases, for a given total planet mass, the presence of a core shrinks the total radius of an EGP. We numerically incorporate such cores into our models by placing a compressible ball of olivine in the center of the model planet. For each model, the core mass (M_c , in Earth masses, as per convention) is set and pressure continuity between the solid core and the gaseous envelope is ensured throughout the evolution. The ANEOS equation of state (Thompson & Lauson 1972) is used for olivine and the Saumon, Chabrier, & Van Horn (1995, SCVH) equation of state is used for the H_2/He envelope. In these calculations, we assume that the specific heat capacity per mole of the solid cores is the same as derived using the

⁹ We assume that the stellar luminosity does not evolve with time.

¹⁰ One Earth mass is equal to 5.98×10^{27} g.

SCVH equation of state. What the actual specific heats and entropies of the core and heavy-element component of the envelope are is an important open issue. If the core has a high thermal inertia, this can delay the cooling of the planet and the shrinkage of its radius. Conversely, if the heat capacity of the core is smaller than that of H/He mixtures, large core models will cool down slightly more quickly than our corresponding models, resulting in slightly smaller planet radii. The zero-pressure density of olivine is $\sim 3.2 \text{ g cm}^{-3}$, significantly higher than the average density of EGPs (Charbonneau et al. 2006a). This is the point. If we replace the olivine with ices or ice/rock mixtures the results vary slightly, but not qualitatively. Reliable equations of state for heavy-element-rich gaseous envelopes that could constitute most of the planet’s mass are still not available, so we assume that these envelopes are dominated by H₂/He mixtures. We have set the helium mass fraction equal to 0.25. Some think that whether the heavy elements are in the core or the envelope, their effect on R_p is the same. This has not been shown, but one can consider the inner core masses with which we deal as substitutes for the total heavy-element burden in the planet. It is the systematics in the group of known transiting planets for which we are looking and the favored parameters of each EGP are bound to improve significantly with time.

Figure 8 plots theoretical total radii as a function of core mass, M_c , for the estimated ages of OGLE-TR-10b, OGLE-TR-56b, HD189733b, and XO-1b (Table 2). These are merely representative. The lines in Fig. 8 are for solar, 3×solar, and 10×solar models. The measured radii of these transiting EGPs are given as dots and the 1- σ radius error bars are indicated with vertical lines. The dots are placed arbitrarily along the horizontal direction at core masses equal to the mass fraction represented by 3×solar metallicity times the total EGP mass and the rightmost extent of the horizontal “error bars” is placed at the corresponding 3×*stellar* metallicity masses. If the central value of the estimated stellar metallicity is below solar (e.g., HD189733b), the horizontal line is truncated at the dot. As Fig. 8 indicates, a core mass of ~ 20 Earth masses can shrink an EGP by $\sim 0.05\text{--}0.1 R_J$. EGPs with smaller total masses (such as for OGLE-TR-10b and HD149026b) manifest a steeper drop in radius with increasing M_c . Also, while only small cores are indicated for XO-1b and HD189733b, for OGLE-TR-10b the core mass derived for an atmospheric metallicity of $\sim 3\times$ solar (if metallicity and opacity were tied) is also the preferred core mass, i.e., the center of the yellow cross intersects the dashed line. This is not often the case in our current model set, since we have decoupled envelope metallicity from atmospheric opacity. However, note that, as Fig. 8 shows, since the intercept of the solar-metallicity lines with the y(radius)-axis is often (though not always) below the radius positions for, e.g., the 3×solar metallicity dots for the dashed 3×solar lines, the increase in the radius due to increasing the metallicity in the atmosphere is often slightly larger than the decrease in the radius due to a possible corresponding increase in the metallicity in the envelope. Moreover, adding ices to constitute a true “ice/rock” core, substituting for the pure olivine core we now assume, should slightly favor larger radii, but we leave this to future studies. So, higher metallicities overall can still be an important part of the solution to the

large-radius problem. Nevertheless, more work on the envelope equation of state for arbitrary heavy-element fractions is still clearly needed.

Table 3 lists in bold the approximate core masses that provide model fits with solar, 3×solar, and 10×solar atmospheres for each of the fourteen EGPs. We have rounded the best-fit core masses to the nearest convenient number. In parentheses in each column, to the left and the right of the bolded values, are the best-fit core masses for radii that are $\pm 1\text{-}\sigma$ from the central radius estimate (Table 1). Hence, the right value is for the larger (+1- σ) radius and the left value is for the smaller (-1- σ) radius. If there is no good fit, or M_c would have had to be negative, we print (\dots). “0” means close to zero, but could be a bit larger. Since we have no age estimates for WASP-1b and WASP-2b, we leave the corresponding rows for them empty in anticipation of future data. For HD149026b, we provide only central estimates and for HD209458b (for which we provide no estimates) the best fits require that the actual transit radius be beyond its 1- σ radius error bars. All these core masses are derived at the central age estimates given in Table 2. Since in most cases these ages are quite uncertain, the actual ages could yield very different core mass estimates. For instance, if an EGP’s age is significantly younger, the predicted radius without a core would be higher (see Figs. 6 and 7). In that case, compensating for the resulting larger radius deficit would require a larger core mass, all else being equal.

We see in Table 3 that larger core masses are required in models with higher atmospheric opacities, with a swing of $\sim 20\text{--}30$ Earth masses from solar to 10×solar. We also see that the range of theoretical values for M_c is very large, from zero to ~ 100 Earth masses. Furthermore, Table 3 suggests that the canonical “15-Earth masses” that works for our solar system giants might be disfavored as the generic giant planet core mass. Moreover, we note that the high- M_p OGLE-TR-132b and the low- M_p HD149026b both require very large cores, though superficially the radius of OGLE-TR-132b might not have seemed anomalous. For HD149026b, with a small M_p , a large F_p , and a small R_p , the conclusion that a large core is required is unexceptional. But for the more massive OGLE-TR-132b, with the highest F_p of the family, it is intriguing that a very large M_c of comparable magnitude may be required. We draw a similar conclusion for OGLE-TR-113b, which is the most massive of the set and has a modest F_p , but may require a core mass of 60-80 Earth masses.

What patterns emerge from this theoretical study and Table 3? Figure 9 plots the parent stellar metallicity versus the theoretical core masses given in Table 3 for twelve of the known transiting EGPs. The different dots for each planet are for the three different atmospheric opacities. In this plot and in Table 3, the dependence of M_c on atmospheric opacity for each of the EGPs is seen to be less important than the wide spread in M_c from object to object. The most important feature to emerge from Fig. 9 is that M_c seems to increase with [Fe/H]. Based upon their preliminary analysis, Guillot et al. (2006) suggest a similar correlation. Those stars with the lowest [Fe/H], such as HD189733, XO-1, HD209458, and the parent of TrES-2, all seem to be orbited by EGPs that require small cores. Those stars with the largest

values of $[\text{Fe}/\text{H}]$, such as OGLE-TR-132 and HD149026, seem to house EGPs that require the largest cores. A “straight” line can be drawn through the points, suggesting a correlation between inferred core mass and stellar metallicity. Moreover, around solar values of the stellar metallicity, the suggested core masses are in the solar-system regime, paralleling Jupiter and Saturn. Finally, on Fig. 9 at low stellar metallicity no large cores are derived, and at high stellar metallicity no small cores are derived. To be sure, there are deviations from this simple picture, such as OGLE-TR-56b and OGLE-TR-10b, but these points are derived using central values of the poorly known ages and stellar metallicities. If the metallicities and/or ages of OGLE-TR-56 and OGLE-TR-10 are slightly lower, the corresponding points will move up and to the left, into the trend line. Similarly, if we derive their core masses using the upper $1\text{-}\sigma$ radii, the corresponding dots will shift upward on Fig. 9. However, it is also not altogether unreasonable to expect some scatter in giant planet formation and in M_c .

On Fig. 9, for each single object one point separately is not very suggestive, but plotted together they collectively indicate a correlation that hints at their origin. At the very least, super-solar and super-stellar heavy-element abundances in the interiors of these planets, if not the presence of cores per se, are strongly suggested. Hence, we offer Fig. 9 as tantalizing evidence for the presence of dense cores and/or heavy-element-rich envelopes in EGPs and, therefore, for the core-accretion model of giant planet formation.

7. EFFECTS OF EXTRA HEAT SOURCE IN INTERIOR

Many workers have sought to explain the large radii of transiting planets such as HAT-P1b, WASP-1b, and HD209458b by invoking an extra power source in the planet’s interior (Bodenheimer, Laughlin, & Lin 2003; Guillot & Showman 2002; Winn & Holman 2005; Chabrier et al. 2004; Charbonneau et al. 2006c). Such a power source would maintain the entropy in the core, and hence its radius, by compensating in part for radiative cooling at its periphery from all quadrants. As our discussions in §5 and §6 indicate, we don’t prefer this solution, and in fact conclude that there are two radius problems, only one of which could be resolved with an extra core heat source. Nevertheless, it is useful to estimate the magnitude of the power required for each transiting EGP to affect its measured radius. The goal is to determine whether the requisite power could be correlated with some other system parameter, such as intercepted stellar power, L_p . In Table 4, we provide such estimates for the transiting EGPs for two cooling models. The first (labeled “Power (Iso)”) ignores stellar irradiation completely and assumes the object can otherwise be considered isolated (see also Chabrier et al. 2004). The central value of the measured radius (Table 1) is assumed to be the target of the fit and ΔR is not added. Solely for the purposes of illustration, the atmospheres have solar opacities. We see in Table 4 that between 0.45% and 0.005% of each EGP’s L_p would be called for. The characteristic variation is a factor of ten. This needed variation from object to object makes unclear the origin of such a power source.

The second model (“Power (Solar)”) also assumes that the atmospheres have solar composition and drops the

ΔR , but includes the effect of stellar irradiation with our default redistribution parameter (§8). These models are the solar-atmosphere/no- ΔR models described in §5, but with an extra power source. In this case, the range of fractions of L_p is more narrow, between 0.01% and 0.05%, and a factor of ten smaller than for the “Power(Iso)” model set, reflecting the effect of irradiation. Note that for more than half the models in this model set an extra heat source would make the radius fit worse, not better. Other atmospheric opacities/metallicities could have been used in this illustrative study, but the qualitative results would have been similar. To further demonstrate the dependence on core power of the evolution of R_p , Figure 10 depicts such trajectories for two representative EGPs, HD209458b and HAT-P1b, for both “Power (Iso)” and “Power (Solar)” assumptions and for a variety of core powers.

While it is noteworthy that the fraction of L_p needed to modify R_p in a measureable way is quite small, no natural mechanism and no systematic reason for significant variation from object to object suggest themselves. Nevertheless, the possibility of an internal power source can not yet be eliminated out of hand. Indeed, such extra heating may emerge as another degree of freedom in the fits. However, at present we find that Occam’s Razor and the arguments in §5 and §6 obviate the necessity for a central role for such an ad hoc core power of undetermined provenance.

We end this section with a curious observation. On Fig. 9, we have placed gold points to indicate the approximate core masses necessary to fit models having an extra internal power source whose magnitude is an arbitrary, fixed, percentage (0.3%) of L_p (the same percentage for all the different L_p s). These models have solar-metallicity atmospheres, but no irradiation or ΔR effects. Even for these models, we see the same general trend of inferred core mass with stellar metallicity that was identified in §6.

8. AMBIGUITY IN COOLING FROM THE DAY/NIGHT SIDES

The day/night difference in the cooling rates of strongly irradiated planets remains the most uncertain aspect of all published theories. If there is no modification of the heat flux at the radiative/convective boundary on the night side due to heat redistribution at depth from the day side, and the planet cools on the night side as if isolated, then the nightside losses will overwhelm the much smaller dayside losses and an extra heat source (§7) may well be required to explain those EGPs with the largest transit radii.

In our default cooling model, we set the redistribution parameter, f , defined in Burrows, Sudarsky, & Hubbard (2003) and Burrows et al. (2004), and used by other groups (e.g., Fortney et al. 2006; Chabrier et al. 2004), equal to $1/4$. This value signifies complete heat redistribution at depth and longitude-independent interior core fluxes outward. The factor, f , influences the day/night temperature(T)/pressure(P) profile contrasts only at high pressures near the radiative/convective boundary (at Rosseland τ_s of $\sim 10^6$; see Burrows et al. 2004). At altitude, the day/night contrast in an EGP’s spectrum, formed at lower Rosseland τ_s of 0.1 to a few, can be large, as suggested by the recent Ups And b light-curve data

(Harrington et al. 2006). However, at the same time, zonal winds at high optical depths can still efficiently redistribute heat and entropy. It is the T/P profile at depth that regulates core cooling. Such efficient deep heat transport is suggested in the work of Showman & Guillot (2002) and Guillot & Showman (2002), but is by no means proven. Nevertheless, we make this assumption in order to discover and explain the systematic features across the family of known transiting EGPs.

As an aside, we note that many people think that rotation is an efficient means to transport heat globally, and use Jupiter and Saturn as examples. There is almost no latitude or longitude dependence of the mid- and far-infrared emissions of either Jupiter or Saturn. Despite the secant effect of the incident stellar flux, their emission temperatures at these wavelengths are almost completely uniform. However, it is not rotation that smooths out these emissions, but the direct heating of the convective regions of these planets by solar infrared (Ingersoll 1976; Hubbard 1977; and Ingersoll and Porco 1978). The radiative/convective boundary is at low optical depths in these solar-system giants. As a result, the solar heat directly absorbed in the convective zone is efficiently redistributed throughout the planet’s interior, setting a uniform inner boundary for internal heat flux outward. For closer-in EGPs, the radiative/convective boundary is at greater depths and this mechanism does not operate. The upshot is that for more strongly-irradiated EGPs, the mechanisms for longitudinal heat transport are more subtle, and problematic. A number of groups are attempting to address this issue with multi-dimensional, though approximate, numerical tools (Menou et al. 2003; Cho et al. 2003; Burkert et al. 2005; Cooper & Showman 2005), but these efforts are only in their early stages.

9. DISCUSSION AND CONCLUSIONS

In this paper, we have calculated the theoretical evolution of the radii of all fourteen of the known transiting giant planets for a variety of assumptions concerning their atmospheric opacities, inner core masses, and possible internal power sources. We have incorporated the effects of stellar irradiation and have customized such effects for each EGP and star. Using measurements of their ages, masses, and transit radii, we have sought to reconcile these transit radii with theory. While it can be difficult to fit each EGP definitively, looking at them collectively can reveal important underlying features of the family as a whole. In doing so, we find that there are two, not one, radius anomalies. Not only are the radii of a subset of the known transiting EGPs larger than expected from previous theory, but many of the other objects are smaller than expected. Unless all the atmospheres have only the default \sim solar-metallicity opacities, the ΔR effect can be ignored, and an internal power source whose magnitude is not correlated in any obvious way with system parameters is operative, we conclude that the spread of measured radii is too large not to admit of a dual problem.

We suggest that the larger EGPs can be explained by invoking enhanced opacity atmospheres, that might be due only in part to enhanced metallicity, that naturally retain internal heat, and, hence, maintain their radii larger, longer. This can be done without an extra internal power source, though such a source can not yet be

eliminated either as an important or a sub-dominant aspect of the theory for some irradiated EGPs. We offer enhanced atmospheric opacities as a more straightforward explanation for the large-radius EGPs. Such an explanation, however, may require non-equilibrium chemistry and/or haze formation in the severe irradiation regimes in which transiting EGPs find themselves and we have not provided in this paper a detailed chemical rationale for such altered atmospheres.

Furthermore, we suggest that the other anomaly, that of the small radii we find for the majority of the known transiting EGPs, can be explained simply by the presence of dense cores and/or metal-rich envelopes in most, or all, of these fourteen objects. For no EGP orbiting a lower-metallicity star do we infer a large inner core. Conversely, for no EGP orbiting the highest-metallicity stars do we infer a small inner core. Moreover, the core masses we find for EGPs transiting near-solar metallicity stars are close to those estimated for Jupiter and Saturn. Importantly, we derive a roughly monotonically-increasing relationship between the stellar metallicity and the estimated core mass. High stellar metallicity has been shown to correlate with the probability of the presence of an EGP in the radial-velocity data (Fischer & Valenti 2005). In this paper, we find that high stellar metallicity may also imply large inner cores and/or metal-rich envelopes. These twin correlations may speak to the mechanism of EGP formation and are in keeping with the core-accretion model of their origin.

There are a number of caveats to our conclusions. First is the uncertainty concerning the nightside cooling. If there is no means by which cooling of the interior can be stanch by heat redistribution at depth from the day-side (Burrows et al. 2004), then an extra power source might be required for the larger radii. Second is the wild card of rotation. Since close-in EGPs are no doubt in synchronous rotation at periods larger than those of Jupiter and Saturn, the effects of rotation will result in no more than a few percent expansion, but have not yet been included in our analysis. Furthermore, centrifugal expansion is most manifest in the transit plane. Third is the possibility of delayed migration of some of the planets. If migration were to take many tens of millions of years (Murray et al. 1998), then the planet might have had time to cool and shrink as if in isolation, without the benefit of the effects of irradiation. Subsequent irradiation when in extremis could not reinflate the core (Burrows et al. 2000). Fourth is the fact that we have merely motivated altered chemistry in the atmospheres of these severely irradiated EGPs, and have not demonstrated the required chemistry, nor the opacity-enhancing effects. High-metallicity atmospheres in themselves would be adequate, but if these were accompanied by envelopes with similar metallicities, the radius-increasing effect can be partially or wholly cancelled. As Fig. 8 demonstrates, in many, though not all, of the cases the enhanced opacity effect of super-solar metallicity in the atmosphere can still trump the shrinkage effect of the same metallicity in the envelope. Super-solar metallicity in the atmosphere, expected generically for EGPs, can still be part of the solution to the large-radius problem. However, in this study we have decoupled the two and future detailed work on UV-driven chemistry, the opacities of strongly irradiated and synchronously-rotating atmo-

spheres, and the equation of state for general mixtures is clearly needed. Fifth is the possibility that the heavy elements and the dominant absorbing compounds of the atmosphere might settle gravitationally, thereby depleting it of its high-opacity components. Without these species, the high-opacity effect that we suggest may be instrumental in explaining the largest EGP radii would be compromised. However, mixing due to the vigorous shear motions caused by the zonal winds anticipated throughout these regions may in fact be adequate to ensure an unstratified atmosphere. Nevertheless, relevant calculations to estimate such mixing are warranted. Finally and sixth are the remaining ambiguities in system age, EGP radius, and stellar metallicity. The inferred core masses, or range of core masses, and the fits to the

larger-radius EGPs depend upon those parameters. Our results could be more robust or less robust, depending upon the eventual values of these quantities.

We thank Maki Hattori, Kat Volk, Christopher Sharp, Mike Cushing, Dimitar Sasselov, and Drew Milsom for helpful discussions and Francis O'Donovan for sharing preliminary data on TrES-2 in advance of publication. We also thank the referee for his careful reading of the manuscript. This study was supported in part by NASA grants NNG04GL22G and NNG05GG05G and through the NASA Astrobiology Institute under Cooperative Agreement No. CAN-02-OSS-02 issued through the Office of Space Science.

REFERENCES

- Alonso, R. et al. 2004, *ApJ*, 613, L153
 Asplund, M., Grevesse, N., & Sauval, A.J. 2006, *Nucl. Phys. A*, 777, 1
 Atreya, S.K., Mahaffy, P.R., Niemann, H.B., Wong, M.H., & Owen, T.C. 2003, *Planet. Space Sci.*, 51, 105
 Atreya, S.K. 2006, in *Proceedings of the International Planetary Probe Workshop, IPPW-4*, Pasadena, CA, June 2006.
 Bakos, G.A. et al. 2006a, *ApJ*, 650, 1160 (astro-ph/0603291)
 Bakos, G.A. et al. 2006b, astro-ph/0609369
 Baraffe, I., Chabrier, G., Barman, T.S., Allard, F., & Hauschildt, P.H. 2003, *A&A*, 402, 701
 Baraffe, I., Chabrier, G., Barman, T.S., Selsis, F., Allard, F., & Hauschildt, P.H. 2005, *A&A*, 436, L47
 Bodenheimer, P., Lin, D.N.C., & Mardling, R.A. 2001, *ApJ*, 548, 466
 Bodenheimer, P., Laughlin, G., & Lin, D.N.C. 2003, *ApJ*, 592, 555
 Boss, A. 1997, *Science*, 276, 1836
 Boss, A. 2001, *ApJ*, 563, 367
 Bouchy, F. et al. 2004, *A&A*, 421, L13
 Bouchy, F. et al. 2005, *A&A*, 444, L15
 Burkert, A., Lin, D.N.C., Bodenheimer, P., Jones, C., & Yorke, H. 2005, *ApJ*, 618, 512
 Burrows, A., Guillot, T., Hubbard, W. B., Marley, M. S., Saumon, D., Lunine, J. I., & Sudarsky, D. 2000, *ApJ*, 534, 97
 Burrows, A., Hubbard, W.B., Lunine, J.I., & Liebert, J. 2001, *Rev. Mod. Phys.*, 73, 719
 Burrows, A., Sudarsky, D. & Hubbard, W.B. 2003, *ApJ*, 594, 545
 Burrows, A., Hubeny, I., Hubbard, W.B., Sudarsky, D., & Fortney, J.J. 2004 *ApJ*, 610, L53
 Cameron, A.C. et al. 2006, astro-ph/0609688
 Chabrier, G., Barman, T., Baraffe, I., Allard, F., & Hauschildt, P.H. 2004, *ApJ*, 603, L53
 Charbonneau, D., Brown, T. M., Noyes, R. W., & Gilliland, R. L. 2002, *ApJ*, 568, 377
 Charbonneau, D., Brown, T.M., Burrows, A., & Laughlin, G. 2006a, to be published in "Protostars and Planets V," ed. B. Reipurth and D. Jewitt (University of Arizona Press), astro-ph/0603376
 Charbonneau, D. et al. 2006b, *ApJ*, 636, 445
 Charbonneau, D., Winn, J.N., Everett, M.E., Latham, D.W., Holman, M.J., Esquerdo, G.A., & O'Donovan, F.T. 2006c, astro-ph/0610589
 Cho, J. Y-K., Menou, K., Hansen, B. M. S., & Seager, S. 2003, *ApJ*, 587, L117
 Cooper, C.S. & Showman, A.P. 2005, *ApJ*, 629, L45 (astro-ph/0502476)
 Fischer, D.A. & Valenti, J. 2005, *ApJ*, 622, 1102
 Flasar, M. et al. 2005, *Science*, 307, 1247
 Fortney, J.J., Sudarsky, D., Hubeny, I., Cooper, C.S., Hubbard, W.B., Burrows, A., & Lunine, J.I. 2003, *ApJ*, 589, 615
 Fortney, J.J., Saumon, D., Marley, M.S., Lodders, K., & Freedman, R.S. 2005, *ApJ*, 642, 495, astro-ph/0507422
 Gillon, M., Pont, F., Moutou, C., Bouchy, F., Courbin, F., Sohy, S., & Magain, P. 2006, *A&A*, 459, 249 (astro-ph/0606395)
 Guillot, T. & Showman, A. P. 2002, *A&A*, 385, 156
 Guillot, T. & Saumon, D. 2004, *ApJ*, 609, 1170
 Guillot, T., Santos, N.C., Pont, F., Iro, N., Melo, C., & Ribas, I. 2006, *A&A*, 453, L21
 Harrington, J., Hansen, B., Luszcz, S., Seager, S., Deming, D., Menou, K., Cho, J., & Richardson, L. 2006, *Science*, 314, 623
 Holman, M.J., Winn, J.N., Stanek, K.Z., Torres, G., Sasselov, D.D., Allen, R.L., & Fraser, W. 2005, astro-ph/0506569
 Holman, M.J. et al. 2006, astro-ph/0607571
 Hubbard, W.B. 1977, *Icarus*, 29, 245
 Hubeny, I. & Lanz, T. 1995, *ApJ*, 439, 875
 Hubeny, I., Burrows, A., & Sudarsky, D. 2003, *ApJ*, 594, 1011
 Ingersoll, A.P. 1976, *Icarus*, 29, 245
 Ingersoll, A.P. & Porco, C.C. 1978, *Icarus*, 35, 27
 Knutson, H., Charbonneau, D., Noyes, R.W., Brown, T.M., & Gilliland, R.L. 2006, astro-ph/0603542
 Konacki, M., et al. 2004, *ApJ*, 609, L37 (astro-ph/0404541)
 Kurucz, R. 1994, *Kurucz CD-ROM No. 19*, (Cambridge: Smithsonian Astrophysical Observatory)
 Laughlin, G., Wolf, A., Vanmunster, T., Bodenheimer, P., Fischer, D., Marcy, G., Butler, P., & Vogt, S. 2005, *ApJ*, 621, 1072
 McCullough, P.R., et al. 2006, *ApJ*, 648, 1228
 Melo, C., et al. 2006, astro-ph/0609259
 Menou, K., Cho, J. Y-K., Hansen, B. M. S., & Seager, S. 2003, *ApJ*, 587, L113
 Moutou, C., Pont, F., Bouchy, F., & Mayor, M. 2004, *A&A*, 424, L31
 Murray, N., Hansen, B., Holman, M., & Tremiane, S. 1998, *Science*, 279, 69
 O'Donovan, F.T. et al. 2006, submitted to *ApJ*, astro-ph/0609335
 Pollack, J.B., Hubickyj, O., Bodenheimer, P., Lissauer, J.J., Podolak, M., & Greenzweig, Y. 1996, *Icarus*, 124, 62
 Pont, F. et al. 2006, submitted to *A&A*(astro-ph/0610827)
 Santos, N.C., Israelian, G., & Mayor, M. 2004, *A&A*, 415, 1153
 Santos, N.C. et al. 2006a, *A&A*, 450, 825
 Santos, N.C. et al. 2006b, astro-ph/0606758
 Sato, B. et al. 2005, *ApJ*, 633, 465
 Saumon, D., Chabrier, G., & Van Horn, H. 1995, *ApJS*, 99, 713
 Showman, A. P. & Guillot, T. 2002, *A&A*, 385, 166
 Shporer, A., Tamuz, O., Zucker, S., & Mazeh, T., 2006, astro-ph/0610556
 Thompson, S.L. & Lauson, H.S. 1972, Sandia National Laboratory Report, SC-RR-71, 0714
 Vaccaro, T. & Van Hamme, W. 2005, *Astrophysics and Space Science*, 296, Numbers 1-4, April, 2005
 Winn, J.N. & Holman, M.J. 2005, *ApJ*, 628, L159
 Winn, J.N., Holman, M., & Fuentes, C.I. 2006, astro-ph/0609471
 Winn, J.N., Holman, M., & Roussanova, A. 2006, astro-ph/0611404

TABLE 1
TRANSITING PLANET DATA¹

Planet	a (AU)	Period (day)	M_p (M_J)	R_p (R_J)	F_p ($10^9 \text{ erg cm}^{-2} \text{ s}^{-1}$)	Ref.
OGLE-TR-56b	0.0225	1.2119	1.29 ± 0.12	1.30 ± 0.05	4.112	1,2,3,4,5
OGLE-TR-113b	0.0229	1.4325	1.32 ± 0.19	1.09 ± 0.03	0.739	1,2,4,6,7,8
OGLE-TR-132b	0.0306	1.6899	1.19 ± 0.13	1.13 ± 0.08	4.528	2,7,9
WASP-2b	0.0307	2.1522	0.88 ± 0.11	1.04 ± 0.06	0.579	10,11
HD 189733b	0.0313	2.2186	1.15 ± 0.04	1.15 ± 0.03	0.468	4,12,13
TrES-2	0.0367	2.4706	$1.28^{+0.09}_{-0.04}$	$1.24^{+0.09}_{-0.06}$	1.150	14
WASP-1b	0.0382	2.5199	0.87 ± 0.07	1.40 ± 0.08	2.488	10,15
TrES-1	0.0393	3.0301	0.75 ± 0.07	1.08 ± 0.3	0.428	1,2,4,16,17
OGLE-TR-10b	0.0416	3.1013	0.63 ± 0.14	1.26 ± 0.07	1.344	1,2,4,5,18
HD 149026b	0.042	2.8766	0.36 ± 0.03	0.73 ± 0.03	2.089	4,19
HD 209458b	0.045	3.5247	0.64 ± 0.06	1.32 ± 0.03	1.074	4,20,21
OGLE-TR-111b	0.047	4.0144	0.52 ± 0.13	1.07 ± 0.05	0.248	1,2,4,22
XO-1b	0.0488	3.9415	0.90 ± 0.07	$1.18^{+0.03}_{-0.02}$	0.485	23,24
HAT-P-1b	0.0551	4.4653	0.53 ± 0.04	$1.36^{+0.11}_{-0.09}$	0.681	25

REFERENCES. — (1) Santos et al. (2006a), (2) Santos et al. (2006b), (3) Vaccaro & Van Hamme (2005), (4) Melo et al. (2006), (5) Pont et al. (2006), (6) Gillon et al. (2006), (7) Bouchy et al. (2004), (8) Konacki et al. (2004), (9) Moutou et al. (2004), (10) Cameron et al. (2006), (11) Charbonneau et al. (2006c), (12) Bouchy et al. (2005), (13) Bakos et al. (2006a), (14) O'Donovan et al. (2006), (15) Shporer et al. (2006), (16) Alonso et al. (2004), (17) Winn, Holman, & Roussanova (2006), (18) Holman et al. (2005), (19) Sato, et al. (2005), (20) Santos, Israelian, & Mayor (2004), (21) Knutson et al. (2006), (22) Winn, Holman, & Fuentes (2006), (23) Holman et al. (2006), (24) McCullough et al. (2006), (25) Bakos et al. (2006b)

^aData, plus representative references, for the fourteen known transiting EGPs with measured M_p and R_p . The list is in order of increasing semi-major axis. F_p is the stellar flux at the planet's substellar point, given the stellar luminosities provided in Table 2.

TABLE 2
DATA ON PARENT STARS¹

Star	Sp.T.	R_* (R_\odot)	T_{eff} (K)	$\log g$ (cgs)	[Fe/H] _*	M (M_\odot)	L_* (L_\odot)	Age (Gyr)	Dist (pc)
OGLE-TR-56	G	1.32 ± 0.06	6119	4.21	0.25	1.04	2.20	$2.5^{+1.5}_{-1.0}$	1600
OGLE-TR-113	K	0.77 ± 0.02	4804	4.52	0.15	0.78	0.29	5.35 ± 4.65	550
OGLE-TR-132	F	1.43 ± 0.10	6411	4.86	0.43	1.35	3.12	1.25 ± 0.75	2200
WASP-2	K1V	0.81 ± 0.03	5200	4.50	...	0.79	0.44
HD 189733	K1.5	0.76 ± 0.02	5050	4.53	-0.03	0.82	0.34	5.25 ± 4.75	19.3
TrES-2	G0V	$1.00^{+0.06}_{-0.04}$	5960	4.40	-0.15	1.08	1.14	$7.2^{+1.8}_{-7.1}$...
WASP-1	F7V	1.42 ± 0.07	6200	4.30	...	1.15	2.67
TrES-1	K0V	0.81 ± 0.02	5226	4.40	0.06	0.88	0.49	4.0 ± 2.0	143
OGLE-TR-10	G	1.16 ± 0.06	6075	4.54	0.28	1.02	1.65	2.0 ± 1.0	1300
HD 149026	G0 IV	1.45 ± 0.10	6147	4.26	0.36	1.3	2.71	2.0 ± 0.8	78.9
HD 209458	G0 V	1.13 ± 0.02	6117	4.48	0.02	1.10	1.60	5.5 ± 1.5	47
OGLE-TR-111	G/K	0.83 ± 0.03	5044	4.51	0.19	0.81	0.40	5.55 ± 4.45	1000
XO-1	G1V	$0.93^{+0.02}_{-0.01}$	5750	4.53	0.015	1.00	0.85	4.6 ± 2.3	200
HAT-P-1	G0V	$1.15^{+0.10}_{-0.07}$	5975	4.45	0.13	1.12	1.52	3.6 ± 1.0	139

^aA compilation of the physical parameters derived for the parents of the known transiting EGPs. The error bars have been rounded from those found in the literature. The ages, the least well-known quantities, should be taken with caution, and those for WASP-1b and WASP-2b, since unpublished, have been omitted. The stellar metallicities are given without error bars, which should be assumed large, and are omitted for WASP-1b and WASP-2b for the same reason their ages are absent. Due to their great distances (rightmost column), the stellar types of the OGLE objects are not well constrained. Refer to Table 1 for the corresponding references.

TABLE 3
APPROXIMATE INFERRED CORE MASS RANGES GIVEN CENTRAL AGE ESTIMATES¹

Planet	Solar	3×Solar	10×Solar	[Fe/H] _*
OGLE-TR-56b	(...) 0 (15)	(0) 10 (25)	(0) 20 (40)	0.25
OGLE-TR-113b	(20) 60 (90)	(40) 70 (115)	(60) 80 (120)	0.15
OGLE-TR-132b	(40) 85 (...)	(75) 100 (...)	(90) 110 (...)	0.43
WASP-2b
HD 189733b	(...) 0 (15)	(0) 5 (25)	(0) 20 (40)	-0.03
TrES-2	(...) 0 (...)	(...) 0 (...)	(0) 15 (...)	-0.15
WASP-1b
TrES-1	(0) 35 (55)	(10) 42 (65)	(20) 55 (70)	0.06
OGLE-TR-10b	(...) 0 (15)	(0) 10 (25)	(0) 20 (40)	0.28
HD 149026b	80	90	110	0.36
HD 209458b	(...) ... (...)	(...) ... (...)	(...) ... (...)	0.02
OGLE-TR-111b	(10) 22 (37)	(13) 27 (42)	(20) 35 (50)	0.19
XO-1b	(...) 0 (...)	(0) 0 (10)	(0) 10 (20)	0.015
HAT-P-1b	(...) ... (...)	(...) ... (...)	(...) ... (5)	0.13

^aThis table provides estimates of the core masses (in Earth masses), or core mass ranges, suggested by our models from the best approximate fits to the measured transit radii. The “best fits” for the measured radii are given in **bold**, while the core masses for $+1\text{-}\sigma$ and $-1\text{-}\sigma$ radii are given in parentheses to the left and right, respectively. When no value is given in parentheses, such a value would be meaningless. For HD149026b, we provide only the central model estimates. Since there are no published values for the ages of WASP-1b and WASP-2b, core mass estimates for them have not been provided. Central values of the stellar metallicity estimates are provide in the last column (see Table 2). As the table headings imply, such estimates depend upon the atmospheric opacities. Since core mass and atmospheric opacity act on the transit radius in opposite senses, the larger the opacity, the larger the core needed to compensate. Remaining large uncertainties in the planet ages, particularly for young ages, and the significant error bars in the planet radii translate into weaker constraints on the core masses than one would like. The upshot is uncertainty and more degrees-of-freedom for the theoretical fits. Nevertheless, this table provides the range and basic systematics in the current family of known transiting EGPs for the cores needed to explain in broad outline the measured transit radii. See the text in §6 for a discussion of the issues involved and some conclusions from this table. See also Fig. 9.

TABLE 4
INTERNAL POWER THAT WOULD BE NECESSARY¹

Planet	Power (Iso) (% L_p)	Power (Solar) (% L_p)	L_p (L_\odot)	F_p (10^9 ergs cm^{-2} s^{-1})
OGLE-TR-56b	0.3	0.05	2.93×10^{-4}	4.112
OGLE-TR-113b	0.02	...	3.63×10^{-5}	0.739
OGLE-TR-132b	0.01	...	2.42×10^{-4}	4.528
WASP-2b	0.005	...	2.62×10^{-5}	0.579
HD 189733b	0.13	...	2.62×10^{-5}	0.468
TrES-2	0.4	0.03	7.42×10^{-5}	1.150
WASP-1b	0.45	0.022	2.04×10^{-4}	2.488
TrES-1	0.025	...	1.95×10^{-5}	0.428
OGLE-TR-10b	0.075	...	8.95×10^{-5}	1.344
HD 149026b	4.61×10^{-5}	2.089
HD 209458b	0.2	0.013	7.86×10^{-5}	1.074
OGLE-TR-111b	0.03	...	1.04×10^{-5}	0.248
XO-1b	0.15	0.01	2.86×10^{-5}	0.485
HAT-P-1b	0.3	0.025	5.29×10^{-5}	0.681

¹Some have suggested that the larger transit radii seen for some EGPs, such as HD209458b, HAT-P1b, WASP-1b, might require an extra internal power source. While not our preferred model (see §7 for a discussion), we provide in this table the power (in percent of the intercepted stellar power, L_p , also given in this table for each EGP) that would be necessary to affect such inflation to the central measured value of the transit radius (Table 1) for two classes of models. As are the other tables, this table is in order of increasing orbital semi-major axis. The first class is for isolated, solar-metallicity, non-irradiated, EGPs (“Power (Iso)”) and the second class is for our solar-metallicity irradiated models (“Power (Solar)”). As can be seen, the latter class of models would require \sim ten times less extra internal power. Also, many EGPs would “require” no (···) extra power, even for solar-metallicity atmospheres. Also provided is the stellar flux (F_p) at the substellar point of the planet (repeated from Table 1). See text in §7 for a discussion.

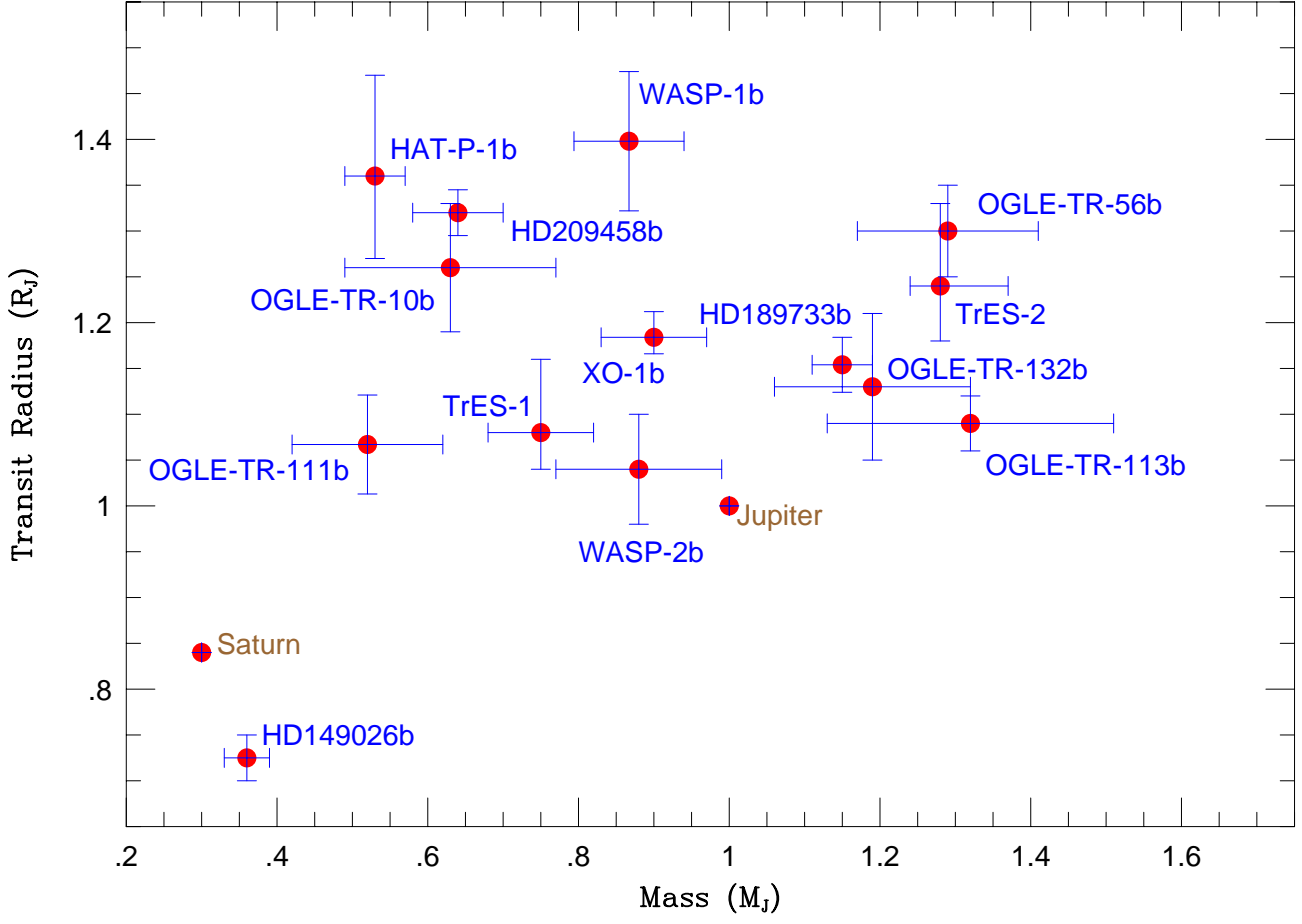


FIG. 1.— Transit radii (R_p , in R_J) of all of the irradiated EGPs listed in Table 1 versus planet mass (M_p , in M_J), along with published $1-\sigma$ error bars for each quantity. For comparison, points for Jupiter and Saturn themselves are also shown.

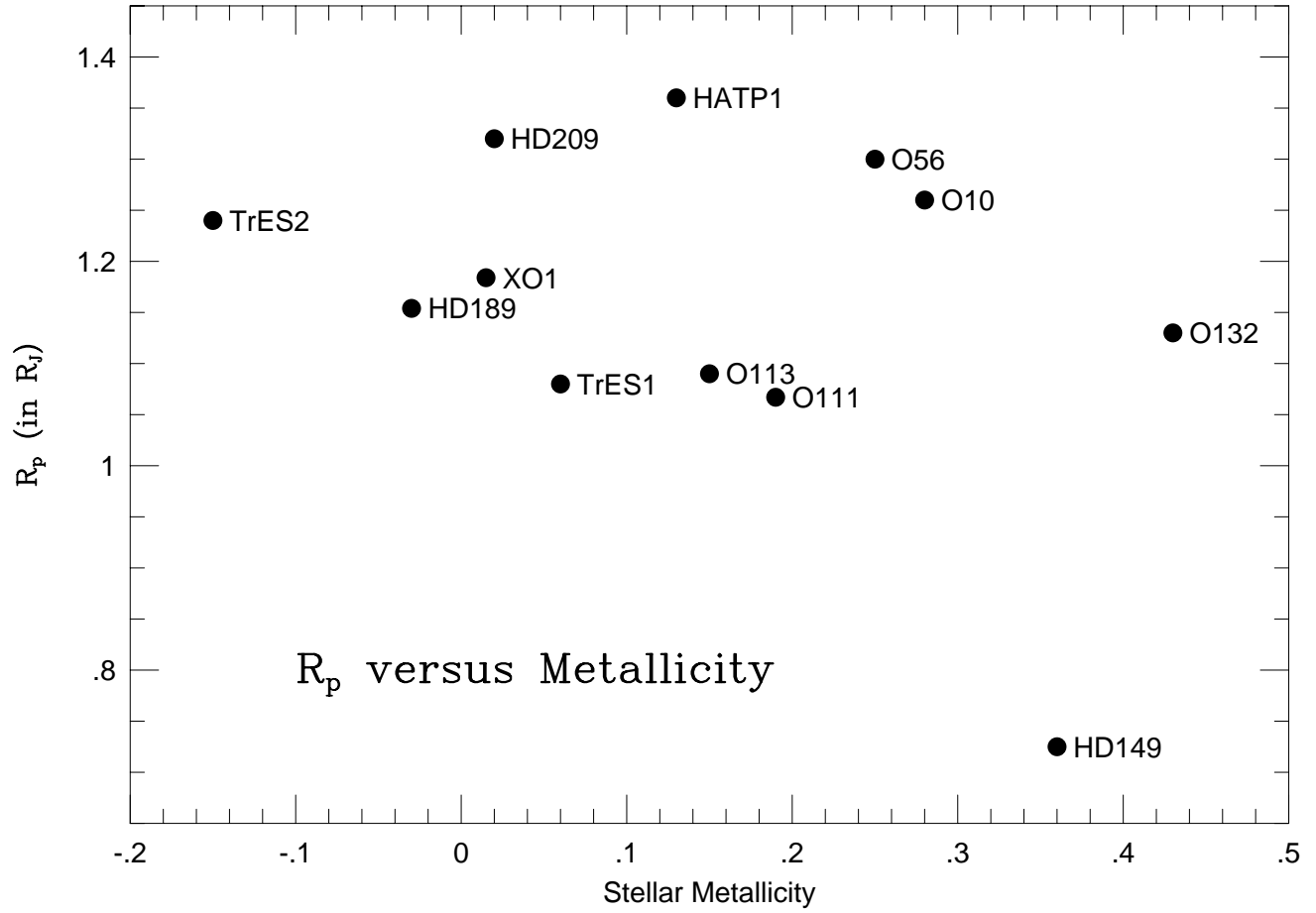


FIG. 2.— Measured planetary radii, R_p (in R_J), versus central values of the estimated stellar metallicities ($[Fe/H]$) of the transiting planets listed in Table 1, except for WASP-1b and WASP-2b for which metallicity estimates have not yet been published. The names for the planets are given in abbreviated form.

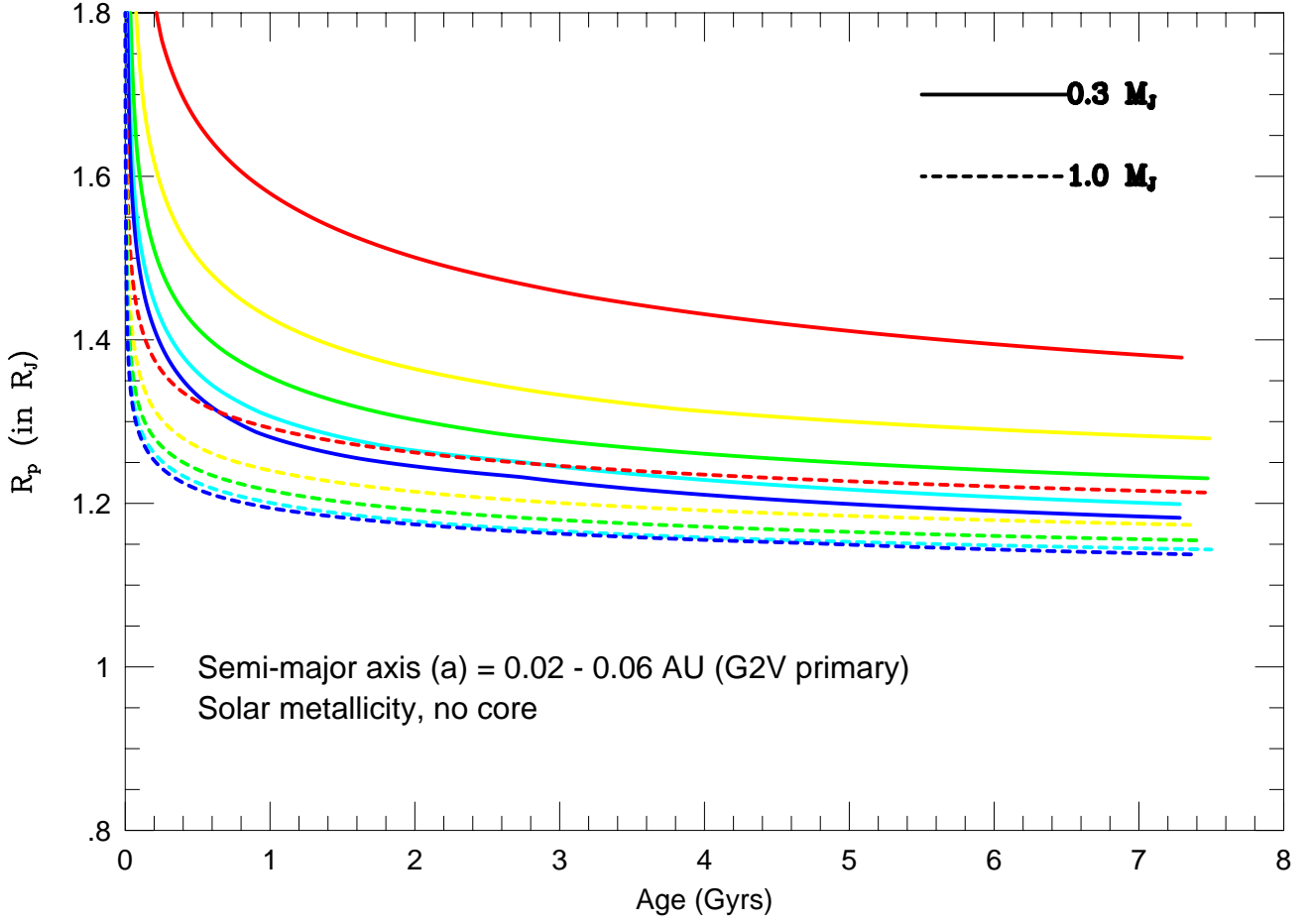


FIG. 3.— R_p (in R_J) versus age (in Gyrs) for model planets with masses of $1 M_J$ (dashed) and $0.3 M_J$ (solid) for different distances [0.02 AU (red), 0.03 AU (yellow), 0.04 AU (green), 0.05 AU (aqua), and 0.06 AU (blue)] from a G2V primary. The models have no cores and assume solar metallicities when calculating the opacities. This plot portrays the systematic dependence of irradiated planet radii with orbital distance for different masses. See text in §3 for a discussion.

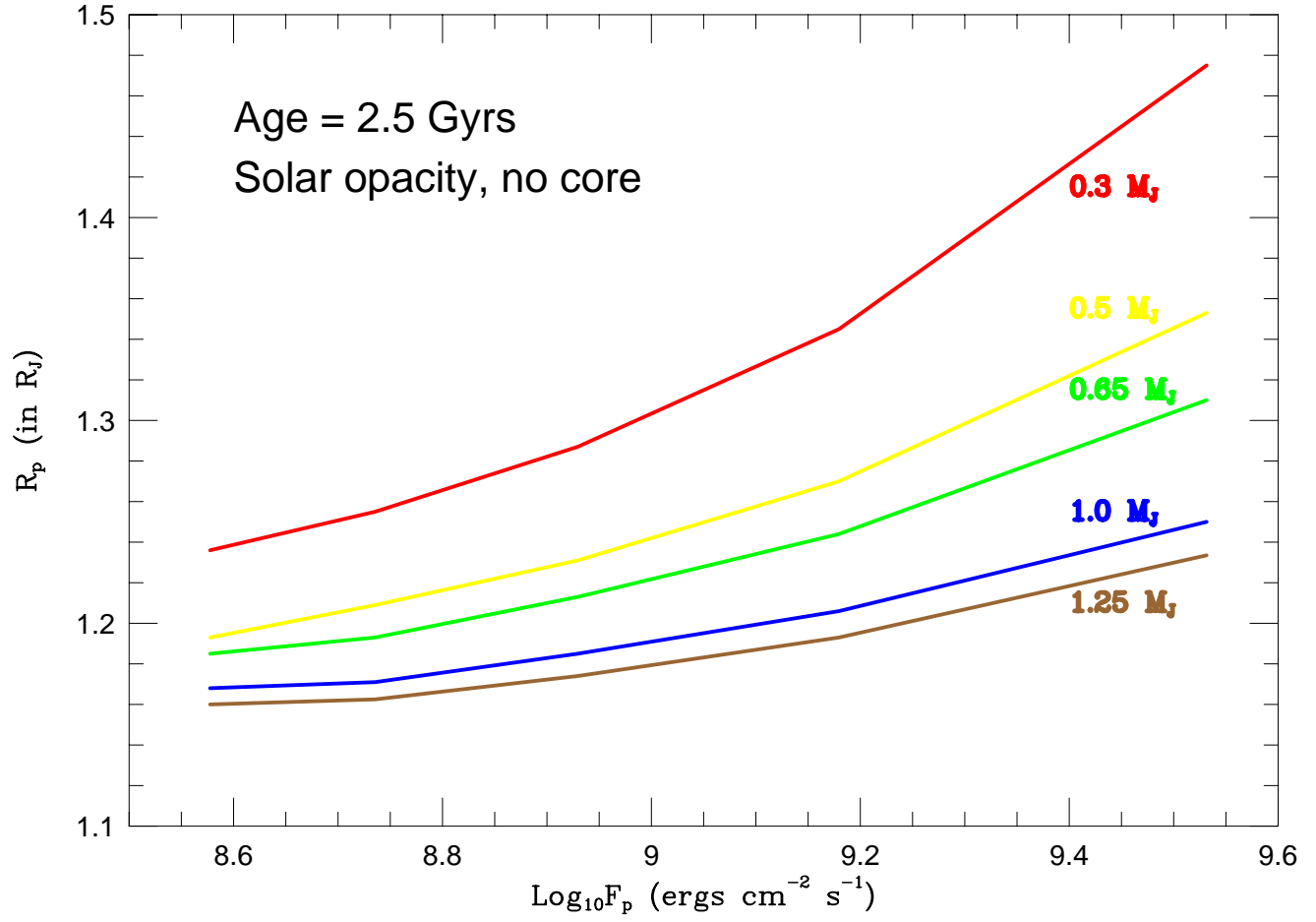


FIG. 4.— Solar-opacity-atmosphere/no-core model radii (R_p , in R_J), at an age of 2.5 Gyr, versus the logarithm base 10 of the stellar flux at the planet (F_p), in units of $\text{erg cm}^{-2} \text{s}^{-1}$, for a range of EGP masses from $0.3 M_J$ to $1.25 M_J$. This figure shows both the planet-mass and the irradiation-flux dependence of the planet radius, at the average age of stars in the solar neighborhood (~ 2.5 Gyr). See text in §3 for a discussion.

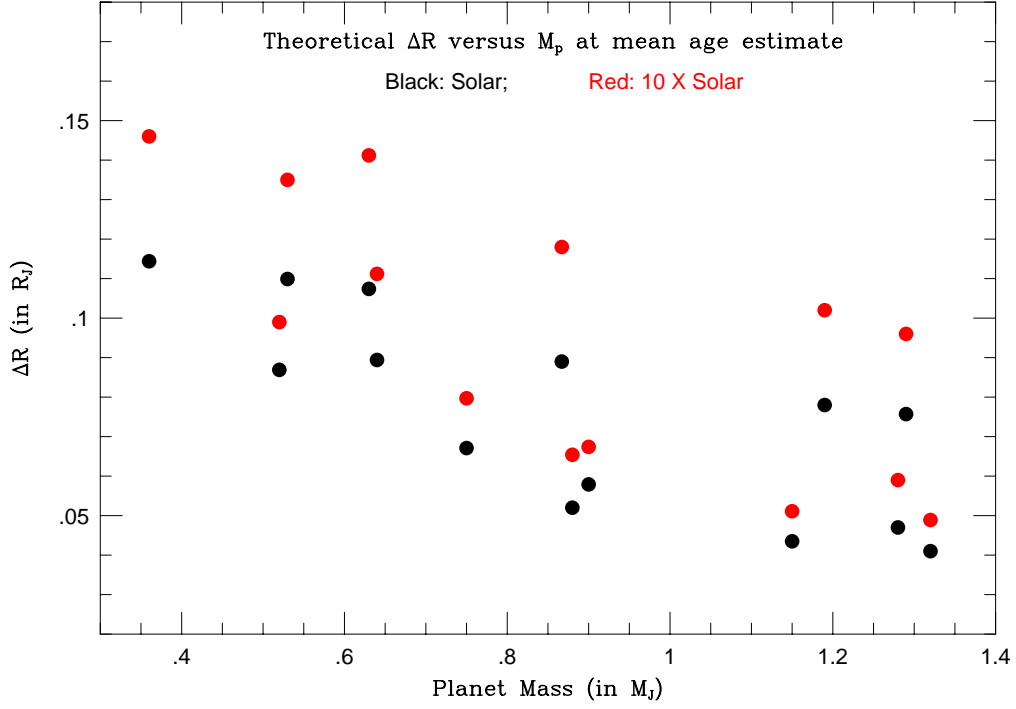


FIG. 5.— The thickness of the radiative zone (ΔR), including the transit radius effect, versus mass for coreless models of twelve of the transiting planets listed in Table 1. The mean molecular weight (μ) used is that for pure H_2/He atmospheres, which is a reasonable approximation if the atmospheric heavy-element abundance is not greatly super-solar. Larger μ s would translate into smaller ΔR s. Since age estimates for WASP-1b and WASP-2b are not published, these objects are not included on this plot. The central values of the putative ages of the planets are assumed and the calculated thicknesses are given for atmospheric opacities at solar (black) and 10×solar (red) atmospheric values. See text in §4 for a discussion.

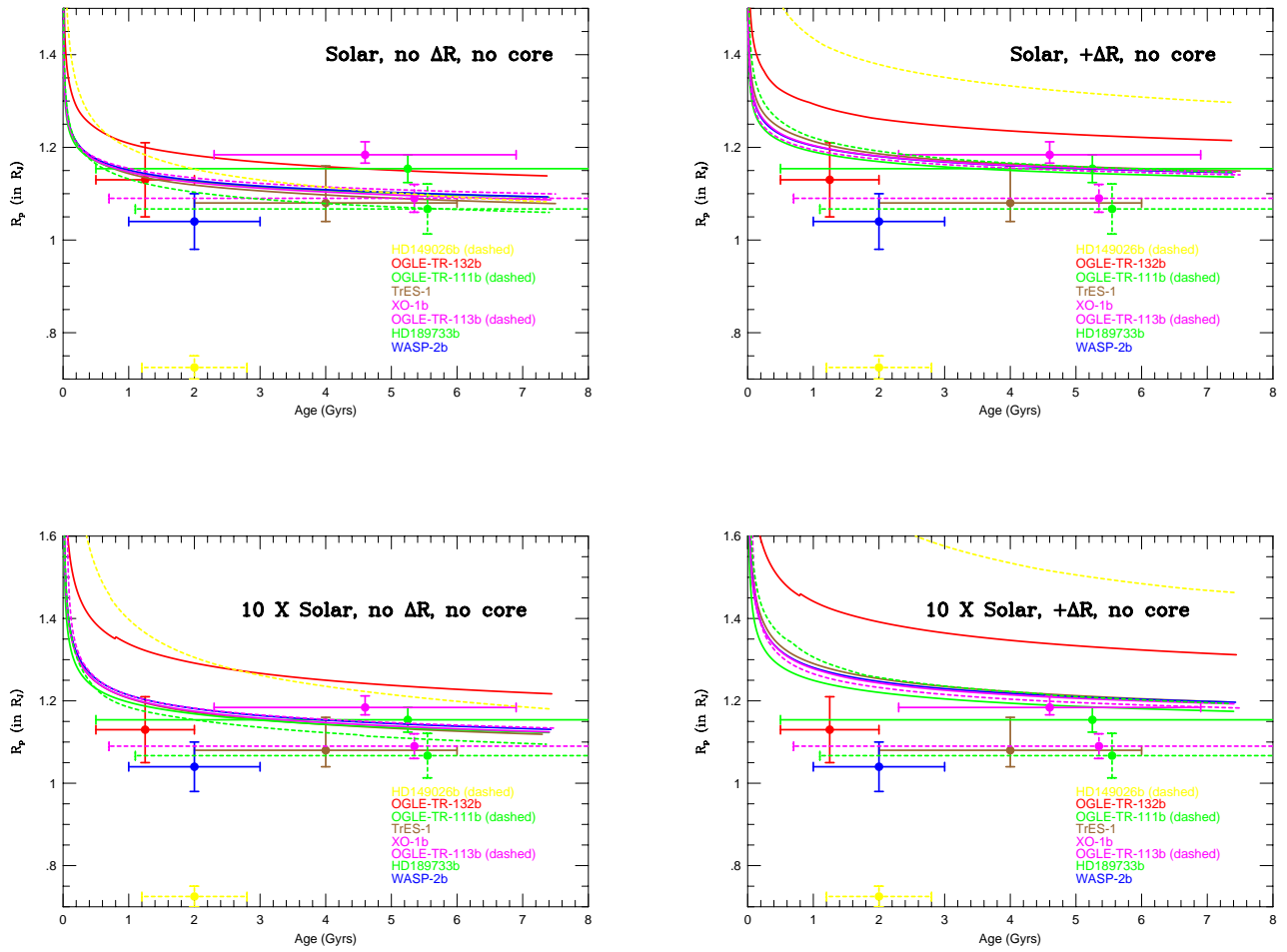


FIG. 6.— R_p (in R_J) versus age (in Gyrs) for a collection of no-core models for the smaller transiting EGPs. They include HD149026b (yellow-dashed), HD189744b (green), OGLE-TR-113b (purple-dashed), OGLE-TR-111b (green-dashed), XO-1b (purple), TrES-1 (gold), WASP-2b (blue), and OGLE-TR-132b (red). The top left panel is for solar opacities and does not include the ΔR term. The top right panel is also solar, but does include the ΔR term. The bottom left panel is for 10x solar opacities, but does not include the ΔR term. The bottom right panel also assumes 10x solar opacities, but does include the ΔR term. This bottom-right panel contains our default no-core/no-cloud models. The age of WASP-2b has been arbitrarily set at 2.0 ± 1.0 Gyrs. The barely-perceptible kinks near ~ 700 Myr in the curves for OGLE-TR-132b (red) at the lower left and right and for OGLE-TR-111b (dashed green) at the lower right are convergence glitches in the evolutionary tracks for those models. See discussion in §5.

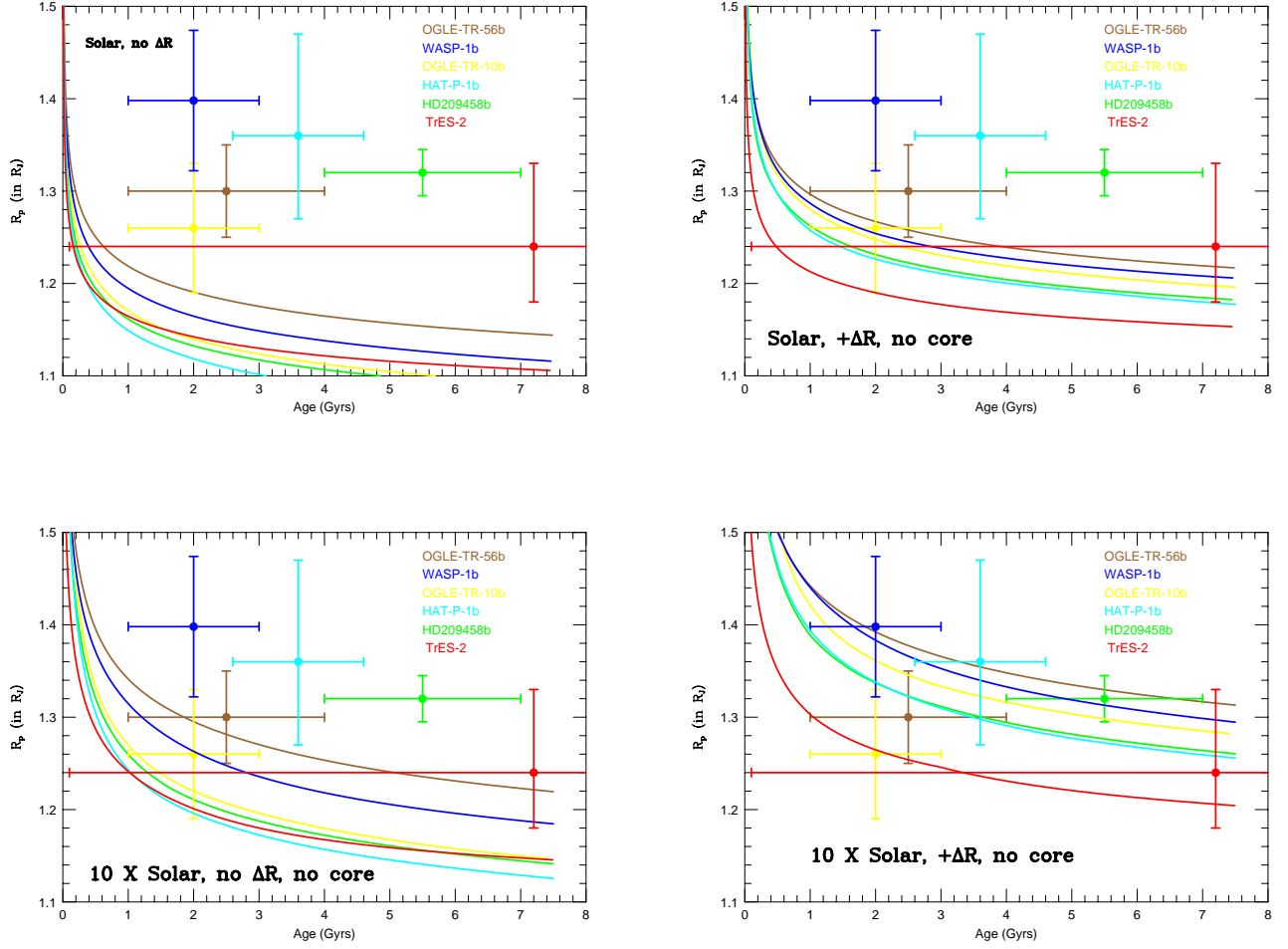


FIG. 7.— R_p (in R_J) versus age (in Gyrs) for a collection of no-core models for the larger transiting EGPs. They include WASP-1b (blue), HATP-1b (aqua), HD209458b (green), TrES-2 (red), OGLE-TR-56b (gold), and OGLE-TR-10b (yellow). As in Fig. 6, the top left panel assumes solar opacities and does not include the ΔR term. The top right panel is also solar opacities, but does include the ΔR term. The bottom left panel is for $10\times$ solar atmospheric opacities, but does not include the ΔR . The bottom right panel also assumes $10\times$ solar opacities, but does include the ΔR term. This bottom-right panel contains our default no-core/no-cloud models. The age of WASP-1b has been arbitrarily set at 2.0 ± 1.0 Gyrs. See §5 for a discussion.

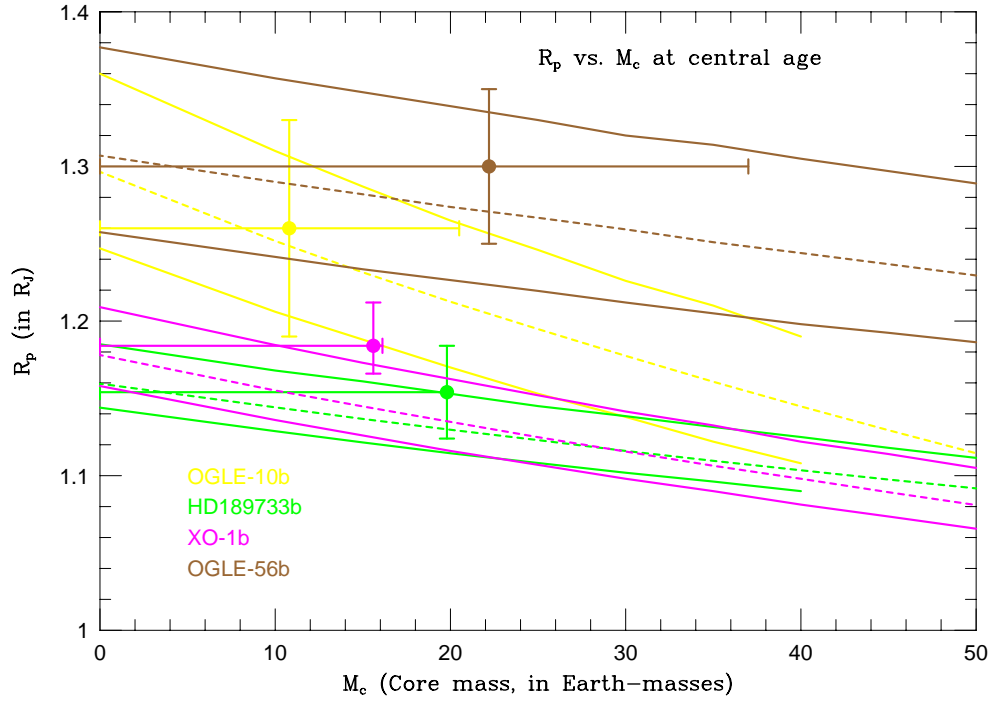


FIG. 8.— Theoretical R_p (in R_J) versus core mass, M_c (in Earth masses), for OGLE-TR-10b (yellow), OGLE-TR-56b (gold), HD189733b (green), and XO-1b (purple). The lines are for solar, 3×solar, and 10×solar atmosphere models and the 3×solar models are dashed. Central values of the estimated stellar ages (Table 2) are assumed. The measured radii of these transiting EGPs, along with 1- σ error bars (vertical), are given. The dots are put arbitrarily at core masses that represent 3×solar metallicity for the given EGP’s measured mass and the rightmost extent of the horizontal “error bars” is placed at 3×*stellar* metallicity masses. If the central value of the estimated stellar metallicity is below solar (as for HD189733b), the line is truncated at the dot. Note that to construct the dots the heavy-element fractions of the atmosphere and of the envelope/core are here set equal. See text in §6 for explanations and a discussion.

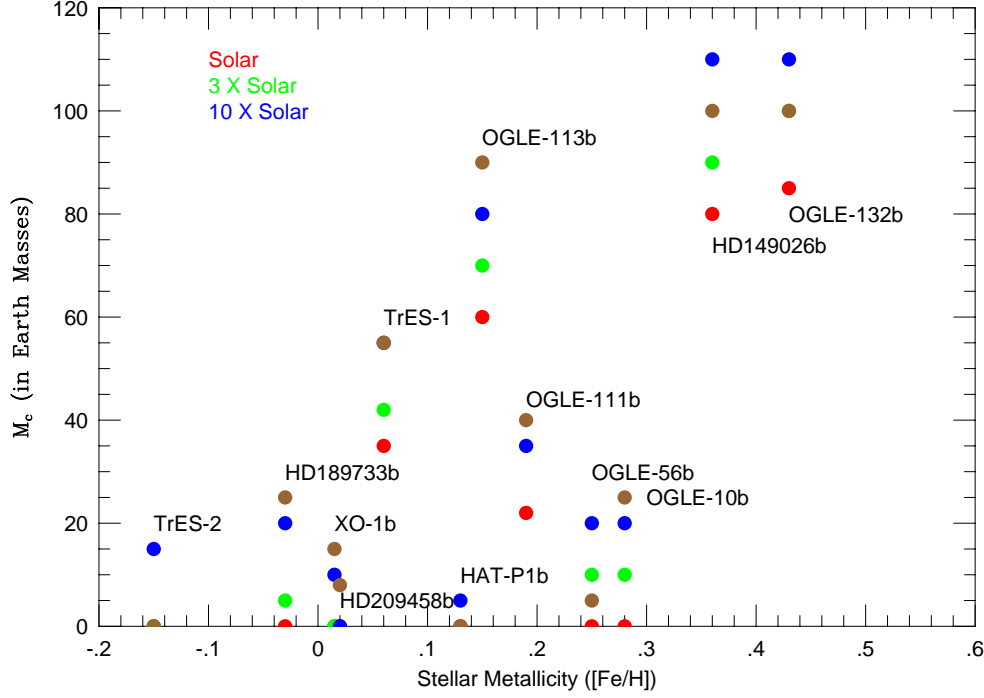


FIG. 9.— Estimated core masses, M_c , (dots, in Earth masses) versus the measured stellar metallicities for twelve of the transiting EGPs listed in Table 1. The values are taken from Table 3, where the mean estimated ages of the systems (Table 2) are assumed. For each EGP, values for solar (red), 3×solar (green), and 10×solar (blue) opacities are given. Since stellar metallicities for WASP-1b and WASP-2b are not published, these EGPs are not included on this plot. Note that despite the clustering at low core masses for the large-radius exemplars (particularly HD209458b and HAT-P1b) and the low core masses for the moderate-stellar-metallicity EGPs OGLE-TR-56b and OGLE-TR-10b, there is a roughly linear (or, better, monotonic) correlation between metallicity and estimated core mass. The gold points indicate the approximate core masses necessary to fit the measured radii when the EGPs in question boast an extra internal power equal to a fixed 0.3% of the corresponding L_p (Table 4). For these last models, solar-opacity atmospheres, but no irradiation or ΔR terms, are presumed, i.e., these are toy isolated models with cores and internal heat sources. See text in §6 and §7 for discussions.

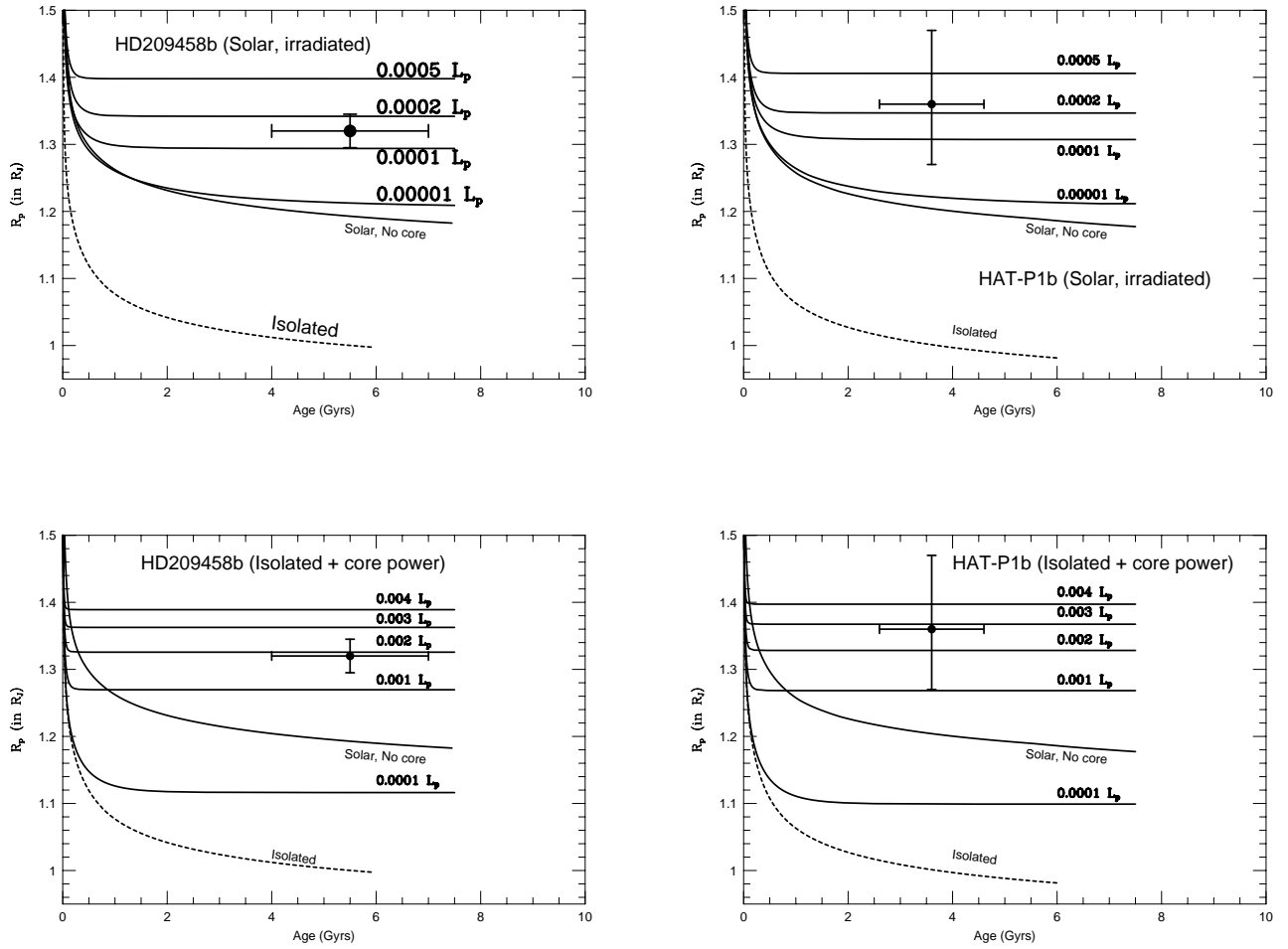


FIG. 10.— **Top:** Theoretical radii of HD209458b (left) and HAT-P1b (right), in units of R_J , versus age (in Gyrs) for different values of an hypothesized core power for irradiated atmospheres with solar-metallicity opacities and no solid inner core. The core power lines are identified by the fraction of L_p , the total stellar power intercepted by the planet. For HD209458b, this is $\sim 7.86 \times 10^{-5} L_\odot$ and for HAT-P1b it is $\sim 5.29 \times 10^{-5} L_\odot$ (Table 4). The dashed lines are evolutionary trajectories for the respective isolated EGPs with solar-metallicity atmospheres without irradiation and without the ΔR term. The lines identified with the words “Solar, No core” are the no-core/irradiated/solar-atmosphere models of Fig. 8. **Bottom:** Same as for the top, but for isolated atmospheres with solar opacities, without irradiation, and with the indicated core powers. Note that the core powers required in this case are much larger than in the irradiated case depicted in the top two panels. See §7 for a discussion.